Amplitude analysis of the $\Xi_c^+ \to pK^-\pi^+$ decay and Ξ_c^+ baryon polarization measurement in semileptonic beauty-hadron decays

R. Aaij *et al.*[*]
(LHCb Collaboration)

(Received 6 August 2025; accepted 7 October 2025; published 7 November 2025)

An amplitude analysis of the $\Xi_c^+ \to pK^-\pi^+$ decay together with a measurement of the Ξ_c^+ polarization vector in semileptonic beauty-hadron decays is presented. The analysis is performed using proton-proton collision data collected by the LHCb experiment, corresponding to an integrated luminosity of 9 fb^{-1}. An amplitude model is developed and the resonance fractions as well as two- and three-body decay parameters are reported. A sizeable Ξ_c^+ polarization is found. A large sensitivity of the $\Xi_c^+ \to pK^-\pi^+$ decay to the polarization is seen, making the amplitude model suitable for Ξ_c^+ polarization measurements in other systems.

DOI: 10.1103/gcft-fgp1

I. INTRODUCTION

The Cabibbo-suppressed $\Xi_c^+ \to pK^-\pi^+$ decay is of special interest for the study of Ξ_c^+ baryon properties due to its clean experimental signature, given by a displaced vertex composed by three quasistable charged hadrons, and a branching fraction of $(0.62 \pm 0.30)\%$ [1]. Cabibbo-favored decays have larger branching fraction values, but they produce long-living hyperons characterized by lower reconstruction efficiencies. This makes the $\Xi_c^+ \to pK^-\pi^+$ decay suitable for the study of Ξ_c^+ baryon properties at the LHCb experiment, and even more at fixed-target experiments, where neutral hyperons have increased their flight distances due to the large Lorentz boost of the Ξ_c^+ baryons produced there.

An amplitude analysis of the $\Xi_c^+ \to pK^-\pi^+$ decay permits the simultaneous determination of the decay amplitudes characterizing intermediate resonant contributions and the measurement of the Ξ_c^+ polarization vector [2]. Such an analysis has diverse applications, ranging from new physics searches to low-energy QCD studies, as described in the following.

The helicity formalism is used to model each contribution to the $\Xi_c^+ \to pK^-\pi^+$ decay, including intermediate-state polarization. The knowledge of the resonant structure is useful in searches for CP-symmetry violation in baryon decays [3–10], as such asymmetries can be related to specific contributions or localized in phase space. Parity violation is characterized by the decay-asymmetry α parameters associated to the two-body resonant contributions, which are determined from the helicity couplings. Parity violation is also studied for the entire three-body $\Xi_c^+ \to pK^-\pi^+$ process, considering a quantity called average event information [11], which represents the sensitivity of the decay to the baryon polarization. The $\Xi_c^+ \to pK^-\pi^+$ decay amplitude model can be exploited in searches for physics contributions beyond the Standard Model in $\Xi_b^0 \to \Xi_c^+ \ell^- \bar{\nu}_\ell$ decays [12–14]. The spin analysis of the Ξ_c^+ baryon in angular analyses of Ξ_b^0 semileptonic decays increases both the number and sensitivity of measurable observables, notably that of the Ξ_c^+ longitudinal polarization.

The $\Xi_c^+ \to pK^-\pi^+$ amplitude model can be employed to measure the polarization of the Ξ_c^+ baryon in multiple production processes. Polarization measurements of charm baryons are a fundamental probe of their spin structure and formation process via hadronization of heavy charm quarks. According to the heavy-quark effective theory, most of the c-quark polarization is expected to be retained by the charm baryon [15–17]. In the case of strong-force production, the baryon polarization is difficult to predict in the nonperturbative regime of QCD, thus its measurement discriminates among different low-energy QCD approaches. Moreover, polarization measurements enable access to charm-baryon electric and magnetic dipole moments via spin precession [18–24]. The measurement of the Ξ_c^+ polarization, in comparison to that of the Λ_c^+ baryon, probes charm-baryon physics in the presence of strangeness.

Neither amplitude analyses of the $\Xi_c^+ \to pK^-\pi^+$ decay, nor Ξ_c^+ polarization measurements, have been performed previously. In this paper, an amplitude analysis of $\Xi_c^+ \to pK^-\pi^+$ decays recorded by the LHCb detector, including the measurement of the Ξ_c^+ polarization vector, is presented. Throughout the paper, charge-conjugate states are

[*]Full author list given at the end of the article.

implied. The analysis is based on a data sample of semileptonic decays of beauty hadrons produced in proton-proton (pp) collisions at center-of-mass energies of 7, 8, and 13 TeV, corresponding to an integrated luminosity of 9 fb^{-1}. The amplitude analysis closely follows the methods employed for the study of the $\Lambda_c^+ \to pK^-\pi^+$ decay at LHCb [25].

This paper is organized as follows. The description of the LHCb detector and the simulation sample employed is given in Sec. II. The selection of $\Xi_c^+ \to pK^-\pi^+$ candidates and the invariant-mass fit used to determine signal and background yields are described in Sec. III. Amplitude and polarization fit frameworks and the development of the $\Xi_c^+ \to pK^-\pi^+$ baseline amplitude model are described in Sec. IV. The evaluation of statistical and systematic uncertainties is covered by Sec. V, along with the consistency checks performed. The results of the amplitude and polarization fits are reported in Sec. VI, and a brief summary of the analysis is provided in Sec. VII.

II. DETECTOR AND SIMULATION

The LHCb detector [26,27] is a single-arm forward spectrometer covering the pseudorapidity range $2 < \eta < 5$, designed for the study of particles containing b or c quarks. The detector includes a high-precision tracking system consisting of a silicon-strip vertex detector surrounding the pp interaction region, a large-area silicon-strip detector located upstream of a dipole magnet with a bending power of about 4 Tm, and three stations of silicon-strip detectors and straw drift tubes placed downstream of the magnet. The tracking system provides a measurement of the momentum, p, of charged particles with a relative uncertainty that varies from 0.5% at low momentum to 1.0% at 200 GeV. Natural units with $c = 1$ are used throughout. The minimum distance of a track to a primary pp collision vertex (PV), the impact parameter, is measured with a resolution of $(15 + 29/p_{\mathrm{T}})$ μm, where p_{T} is the component of the momentum transverse to the beam, in GeV. Different types of charged hadrons are distinguished using information from two ring-imaging Cherenkov detectors. Photons, electrons and hadrons are identified by a calorimeter system consisting of scintillating-pad and preshower detectors, an electromagnetic and a hadronic calorimeter. Muons are identified by a system composed of alternating layers of iron and multiwire proportional chambers.

The online event selection is performed by a trigger, which consists of a hardware stage, based on information from the calorimeter and muon systems, followed by a software stage, which applies a full event reconstruction. At the hardware trigger stage, events are required to have at least one muon with high p_{T}. The software trigger requires a two-, three- or four-track secondary vertex with a significant displacement from any primary pp interaction vertex. At least one charged particle must have a transverse momentum $p_{\mathrm{T}} > 1.6$ GeV and be inconsistent with originating from a PV. A multivariate algorithm [28,29] is used for the identification of secondary vertices consistent with the decay of a b hadron.

The momentum scale is calibrated using samples of $J/\psi \to \mu^+\mu^-$ and $B^+ \to J/\psi K^+$ decays collected concurrently with the data sample used for this analysis [30,31]. The relative accuracy of this procedure is estimated to be 3×10^{-4} using samples of other b hadrons, Υ and K_{S}^0 mesons.

Simulation is required to model the effects of the detector acceptance and the imposed selection requirements. In the simulation, pp collisions are generated using PYTHIA [32] with a specific LHCb configuration [33]. Decays of unstable particles are described by EvtGen [34], in which final-state radiation is generated using PHOTOS [35]. The interaction of the generated particles with the detector, and its response, are implemented using the Geant4 toolkit [36] as described in Ref. [37]. The underlying pp interaction is reused multiple times, with an independently generated signal decay for each [38].

A sample of exclusive semileptonic $\Xi_b^0 \to \Xi_c^+\mu^-\bar{\nu}_\mu$ decays is produced with the $\Xi_c^+ \to pK^-\pi^+$ decay uniformly generated over the phase space. These simulated decays permit a suitable description of detector efficiency effects, despite the fact that other beauty-hadron decays could, in principle, contribute to the decay under study. The particle identification (PID) response in the simulated samples is calibrated by sampling from data distributions of $D^{*+} \to D^0\pi^+$, $D^0 \to K^-\pi^+$ and $\Lambda_b^0 \to \Lambda_c^+\pi^-$, $\Lambda_c^+ \to pK^-\pi^+$ decays, considering their kinematics and the detector occupancy. An unbinned method is employed, where the probability density functions are modeled using kernel density estimation [39]. Simulated distributions are validated on data, correcting observed differences using the gradient-boost weighting technique of the HEP_ML package [40].

III. EVENT SELECTION AND INVARIANT-MASS FIT

Data used in this analysis are split into a Run 1 dataset comprising pp collisions recorded at center-of-mass energies of 7 TeV and 8 TeV, and a Run 2 dataset recorded at 13 TeV center-of-mass energy. They correspond to integrated luminosities of approximately 3 fb^{-1} and 6 fb^{-1}, respectively. The two datasets are treated in the same way but analyzed separately to consider possible differences due to the different data-taking conditions.

The Ξ_c^+ candidates are reconstructed from combinations of three charged hadron tracks forming a vertex separated from any PV. Semileptonic beauty-hadron decay candidates are then reconstructed inclusively requiring that the Ξ_c^+ candidate and a muon track originate from a common vertex. Small χ^2 values are required for all track and vertex fits. Each track is required to have a loose PID response;

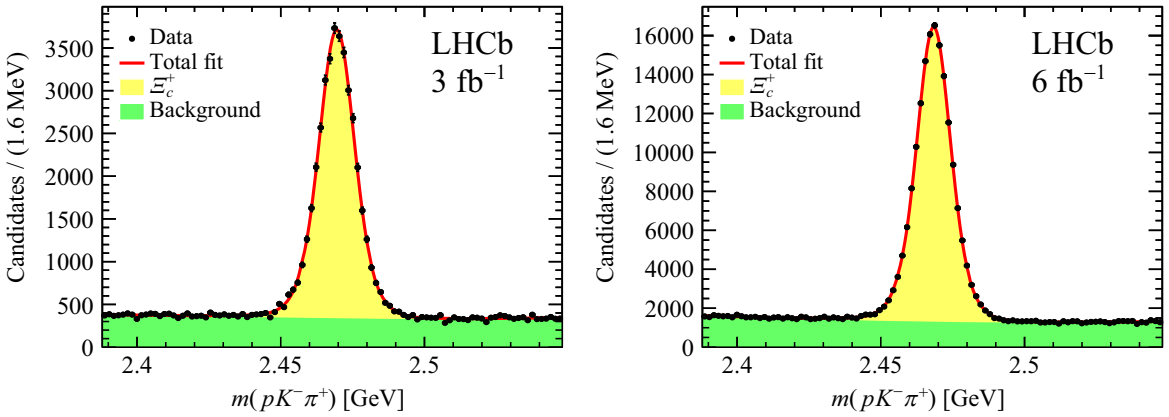

FIG. 1. Distributions of the $pK^-\pi^+$ invariant mass of (left) Run 1 and (right) Run 2 selected candidates. The results from the fit described in the text are also shown.

transverse momentum $p_T > 250$ MeV for hadrons and $p_T > 1$ GeV for muons; and momentum $p > 2$ GeV for mesons, $p > 8$ GeV for protons and $p > 6$ GeV for muons. Final-state particles are ensured to be well displaced from the interaction point by requiring a large track χ^2_{IP} with respect to any PV, where χ^2_{IP} is defined as the difference in the vertex fit χ^2 of a given PV reconstructed with and without the particle under consideration. The PV with the smallest χ^2_{IP} is associated to the Ξ_c^+ candidate.

A set of selection criteria are imposed to reduce the combinatorial background, arising from random combinations of tracks. They require each track to be within the LHCb detector pseudorapidity acceptance, $2 < \eta < 5$, and maximum decay times of 3 ps and 10 ps for Ξ_c^+ and beauty-hadron candidates, respectively. Requirements are imposed also on proton and kaon PID probabilities, obtained from neural network classifiers, which combine information from the different subdetectors [41].

A boosted decision tree (BDT) classifier [42] is used to further reduce the combinatorial background contamination. The classifier is trained on data passing the aforementioned selection criteria, with signal and background proxies obtained via an *sPlot* technique [43], separately for Run 1 and Run 2 datasets. It employs quantities related to decay topology, track fit quality, PID and the proton transverse momentum. A selection cut on the BDT classifier output is chosen optimizing the figure of merit $N^2/(N+B)^{3/2}$, with N and B the signal and background yields. These are obtained in the $m(pK^-\pi^+)$ signal region within ± 15 MeV of the known Ξ_c^+ mass [1], covering approximately three times the mass-peak resolution.

The three-body charm-meson decays $D^+ \to K^-\pi^+\pi^+$, $D_s^+ \to K^-K^+\pi^+$ and $D^+ \to K^-K^+\pi^+$ constitute the main physical background contributions. They are identified by considering events with invariant mass reconstructed under the $\pi^+K^-\pi^+$ hypothesis within ± 15 MeV of the known D^+ mass or invariant mass reconstructed under the $K^+K^-\pi^+$ hypothesis within ± 15 MeV of the known D^+ or D_s^+ masses. These events are then discarded only if the proton PID probability is lower than a given threshold. This requirement allows a more uniform efficiency over the $\Xi_c^+ \to pK^-\pi^+$ decay phase-space distributions while maintaining an adequate background rejection. Other physical background contributions are negligible after the selection process. A background contribution originating from events in which the same positive track is reconstructed as a proton and a pion at the same time is removed by rejecting candidates in which the proton and pion momenta point in the same direction, i.e., with relative angle difference below 10^{-3}.

The distribution of the invariant mass $m(pK^-\pi^+)$ of selected candidates from the Run 1 and Run 2 datasets is shown in Fig. 1. Extended unbinned maximum-likelihood fits are performed in the mass range within ± 80 MeV of the known Ξ_c^+ mass, to determine $\Xi_c^+ \to pK^-\pi^+$ and background yields after selection. The $\Xi_c^+ \to pK^-\pi^+$ signal shape except for the overall mean and width is fixed from simulation, while a polynomial function describes the combinatorial background contribution.

The signal $m(pK^-\pi^+)$ region chosen for the amplitude analysis is within ± 15 MeV of the known Ξ_c^+ mass, containing 99.7% of the signal candidates. Yields for the Run 1 and Run 2 data samples of 35,265 and 151,887 $\Xi_c^+ \to pK^-\pi^+$ candidates are found, with background fractions in the signal region (f_b) at 15.6% and 14.4%, respectively.

IV. AMPLITUDE AND POLARIZATION FITS

The amplitude model for the $\Xi_c^+ \to pK^-\pi^+$ decay is written in the helicity formalism [44], following the method and conventions of Ref. [45]. The Ξ_c^+ polarization is measured in the Ξ_c^+ rest frame in two different helicity systems defined by a boost along the Ξ_c^+ momentum from the approximate beauty-hadron rest frame ($\tilde{B}$) and from the laboratory frame (*lab*). The five variables describing the $\Xi_c^+ \to pK^-\pi^+$ decay phase space are chosen to be

$$\Omega \equiv (m^2(pK^-),\ m^2(K^-\pi^+), \cos\theta_p, \phi_p, \chi), \qquad (1)$$

where $m^2(pK^-)$ and $m^2(K^-\pi^+)$ are the squared invariant masses and θ_p, ϕ_p, and χ are the angles describing the decay orientation with respect to the Ξ_c^+ polarization system. The angles θ_p and ϕ_p are the polar and azimuthal angles of the proton momentum, while χ is the angle between the plane formed by the proton momentum and the Ξ_c^+ quantization axis, and the plane formed by the kaon and pion momenta, where momenta are expressed in the Ξ_c^+ rest frame. The phase-space variables are computed after constraining the mass of the $pK^-\pi^+$ candidate to the known Ξ_c^+ mass. The detailed definition of the amplitude model, Ξ_c^+ helicity systems and phase-space variables is given in Ref. [25].

The free parameters of the amplitude model are determined by an unbinned maximum-likelihood fit to the five phase-space observables. The detector efficiency effects on the $\Xi_c^+ \to pK^-\pi^+$ phase space are included using calibrated simulation events passing event selection, while the background contribution is introduced using factorized Legendre-polynomial expansions, derived from data mass sidebands. Their distributions represent reliably the background contribution in the signal region since phase-space variables are mostly uncorrelated with the invariant mass $m(pK^-\pi^+)$. The maximum-likelihood fit is performed simultaneously on the separate Run 1 and Run 2 datasets, using specific simulation samples and background parametrizations for each dataset.

The amplitude fitting code is based on a version of the TensorFlowAnalysis package [46] adapted to three-body amplitudes in five-dimensional phase-space fits [21]. This package depends on the machine-learning framework TensorFlow [47] interfaced with Minuit minimization [48] via the ROOT package [49]. The fit is performed using multiple gradient-descent minimization with different, randomized, initial values of the parameters to ensure that the best fit point in parameter space is reached.

The fit quality is measured by a χ^2 test performed over a five-dimensional binning of the phase space; an adaptive binning technique is employed to guarantee a similar number of candidates in each bin. Probability values are obtained assuming a number of degrees of freedom equal to the number of bins employed minus the number of free parameters in the amplitude fit, including normalization.

The normalization of the model is determined by setting the complex coupling $\mathcal{H}_{1/2,0}^{\bar{K}^*(892)^0}$ to (1,0), with the values of the other couplings expressed relative to this reference. The baseline model is obtained from the amplitude fit in which the Ξ_c^+ polarization is expressed in the helicity system reached from the $\tilde{B}$ rest frame. All the helicity couplings of the intermediate resonances are measured in the present analysis. Fit fractions and decay-asymmetry parameters are also determined for each two-body contribution. In light of the application of the $\Xi_c^+ \to pK^-\pi^+$ amplitude model as a Ξ_c^+ polarization analyzer, the sensitivity of the decay to the baryon polarization is measured by the normalized average event information, $\sqrt{3}S$, defined in Ref. [25]. This quantity depends on the parity-violating part of the decay rate, and is inversely proportional to the variance of the polarization measurement. The $\sqrt{3}S$ quantity is also measured for the nonzero-spin K^* states in place of their decay-asymmetry parameters.

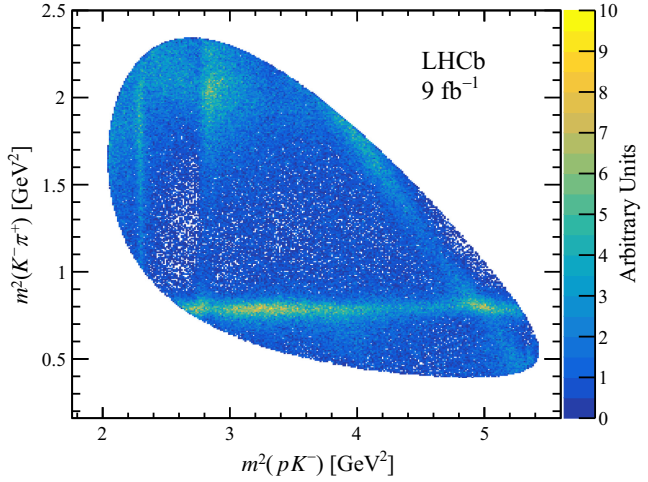

FIG. 2. Dalitz plot for the total sample of selected $\Xi_c^+ \to pK^-\pi^+$ candidates. The sample consists of 187,152 candidates with a purity of 85.4%.

A Dalitz plot of the total reconstructed $\Xi_c^+ \to pK^-\pi^+$ sample is presented in Fig. 2. The plot contains candidates from the signal region prior to efficiency correction, drawn in the $m^2(pK^-)$ and $m^2(K^-\pi^+)$ squared invariant masses. It displays a rich structure with resonant contributions from all three possible pairs of final state particles; Λ resonances are visible as vertical bands, $\bar{K}^*$ as horizontal bands and Δ^{++} as diagonal bands. The different intensity patterns can be explained by the spin of the resonance within each band, by interference patterns where bands overlap, or nonuniform detector efficiency near the boundaries of phase space.

The baseline amplitude model is built starting from the contributions visible in Fig. 2 and adding resonant states according to those listed in Ref. [1]. Contributions which significantly improve the fit quality are added to the baseline model; those giving similar qualities are considered as alternative models for the evaluation of systematic uncertainties. The same criterion is employed for choosing among different descriptions of the same contribution. The resonances included in the baseline model are listed in Table I, where their invariant-mass dependence (lineshape) follows that of Ref. [25]. Resonances are parametrized by default with relativistic Breit-Wigner functions multiplied by orbital angular-momentum-suppression terms. The $\Lambda(1405)$ and $\Lambda(1670)$ resonances are parametrized by a Flatté lineshape [50]. Spin-zero $K^-\pi^+$ contributions, i.e.,

TABLE I. Resonant composition of the baseline $\Xi_c^+ \to pK^-\pi^+$ amplitude model, with spin-parity J^P, and the Breit-Wigner mass and width parameters.

Resonance	J^P	Mass [MeV]	Width [MeV]	Reference
$\Lambda(1405)$	$1/2^-$	1405.1	50.5	[1]
$\Lambda(1520)$	$3/2^-$	1518.467	15.195	[25]
$\Lambda(1600)$	$1/2^+$	1600	200	[1]
$\Lambda(1670)$	$1/2^-$	1674.4	27.2	[52]
$\Lambda(1690)$	$3/2^-$	1690	70	[1]
$\Lambda(1710)$	$1/2^+$	1713	180	[1]
$\Lambda(1800)$	$1/2^-$	1800	200	[1]
$\Lambda(1810)$	$1/2^+$	1790	110	[1]
$\Lambda(1820)$	$5/2^+$	1820	80	[1]
$\Lambda(1830)$	$5/2^-$	1825	90	[1]
$\Lambda(1890)$	$3/2^+$	1890	120	[1]
$\Lambda(2000)$	$1/2^-$	1988.19	179.26	[25]
$\bar{K}_0^*(700)^0$	0^+	845	468	[1]
$\bar{K}^*(892)^0$	1^-	895.5	47.3	[1]
$\bar{K}_0^*(1430)^0$	0^+	1425	270	[1]
$\bar{K}_2^*(1430)^0$	2^+	1432.4	109	[1]
$\Delta(1232)^{++}$	$3/2^+$	1232	117	[1]
$\Delta(1600)^{++}$	$3/2^+$	1570	250	[1]
$\Delta(1620)^{++}$	$1/2^-$	1610	130	[1]
$\Delta(1700)^{++}$	$3/2^-$	1665	250	[1]

$\bar{K}_0^*(700)^0$ and $\bar{K}_0^*(1430)^0$ states, are effectively described by a simplified version of the parametrization proposed in Ref. [51]. It consists of a Breit-Wigner lineshape in which the mass-dependent width is given by

$$\Gamma(m) = \frac{m^2 - s_A}{m_0^2 - s_A}\Gamma_0 e^{-\gamma m^2}, \tag{2}$$

which features a singularity (Adler zero) at $s_A = m_K^2 - 0.5m_\pi^2$ and an exponential form factor on the $K\pi$ width driven by the parameter γ. The γ parameter is determined separately for each contribution in the amplitude fit, with mass m_0 and width Γ_0 Breit-Wigner parameters taken from Ref. [1]. The effect of this choice is taken into account in the computation of the model systematic uncertainty, described later, by releasing mass and width parameters in the fit, by varying the PDG values for the masses and widths by one standard deviation, and by considering relativistic Breit-Wigner functions as an alternative lineshape. All resonance parameters are fixed to the mean values reported in Ref. [1] except for the $\Lambda(1520)$ and $\Lambda(2000)$ states, which are fixed to the central values determined by the $\Lambda_c^+ \to pK^-\pi^+$ amplitude analysis [25], and for the $\Lambda(1670)$ resonance, which are fixed to the values determined by the Belle Collaboration [52]. While no clear contribution of Σ^0 states is found, their possible presence is considered among alternative models. The phase-space distributions are fully described by resonant contributions, with no need for additional nonresonant terms.

The Ξ_c^+ polarization in the $\tilde{B}$ system is determined directly by the amplitude fit, while that in the *lab* system is measured via a separate fit in which the amplitude-model parameters are fixed to those determined in the other polarization system. This strategy, different with respect to that employed for the $\Lambda_c^+ \to pK^-\pi^+$ analysis [25], is motivated by the higher level of background contributions affecting the $\Xi_c^+ \to pK^-\pi^+$ decay channel. In particular, charm-meson decays produce peaking structures in the *lab* system $\cos\theta_p$ distribution. The effect on *lab* system polarization due to the removal of this background source, which distorts the $\cos\theta_p$ distribution, is corrected for by exploiting both the simulation sample and the amplitude model determined in the $\tilde{B}$ frame.

V. UNCERTAINTIES AND CONSISTENCY CHECKS

Statistical and systematic uncertainties are computed for amplitude-model parameters, polarization components, fit fractions, decay-asymmetry parameters and S^2 quantities. Statistical uncertainties are obtained by fitting the baseline model to 1000 pseudoexperiments sampled from fit results. For each pseudoexperiment, the simulation sample used to compute the model normalization is also regenerated to account for its finite size. Two separate studies are performed for the amplitude fit, with polarization measured in the $\tilde{B}$ system, and for the *lab* system polarization-only fit. Statistical uncertainties for each parameter are determined as the standard deviation of the distribution of results from the pseudoexperiments, reported along with the final results in Sec. VI.

Different sources of systematic uncertainties are considered. These are grouped into contributions coming from the model choice, the background determination, kinematics of the decay, PID, and the fit bias. For the *lab* polarization fit, an additional contribution for the correction related to the removal of charm-meson decays is considered. The model contribution is quoted separately from the other experimental systematic contributions, which are combined in the final results.

The systematic uncertainty associated to the amplitude model choice is estimated by determining the measured parameters employing alternative models with fit quality similar to the baseline fit, which is the best representation of the resonant structure of the $\Xi_c^+ \to pK^-\pi^+$ decay. Alternative models cover different types of baseline fit modifications. They include allowing the Breit-Wigner parameters of resonances with sizeable uncertainties to vary freely. Particular attention is given to the spin-zero $K^-\pi^+$ resonances, whose parameters are either floated or shifted by one standard deviation according to the PDG uncertainty intervals. Alternative scenarios also explore the

TABLE II. Systematic uncertainty contributions on polarization components in percentage. Total* includes all contributions except for the choice of amplitude model. Veto refers to the contribution connected to the removal of charm-meson decays.

Parameter	Model	Total*	Background	Kinematics	PID	Veto	Fit bias
P_x $(\tilde{B})$	0.011	0.009	0.007	0.004	0.001		<0.001
P_y $(\tilde{B})$	0.0023	0.0035	0.0019	0.0023	0.0018		0.0001
P_z $(\tilde{B})$	0.028	0.015	0.015	<0.001	<0.001		0.002
P $(\tilde{B})$	0.030	0.016	0.016	0.002	<0.001		0.002
P_x (lab)	0.026	0.010	0.009	<0.001	0.003	0.002	<0.001
P_y (lab)	0.0019	0.0023	0.0002	0.0006	0.0015	0.0017	0.0001
P_z (lab)	0.014	0.020	0.007	0.007	0.014	0.010	<0.001
P (lab)	0.030	0.012	0.010	0.003	0.003	0.006	<0.001

removal of the $\Lambda(1800)$ and $\Lambda(1890)$ states, which exhibit limited statistical significance in the fit. Their exclusion has no observable impact on the remaining resonant structure, although a significant change in the likelihood is observed when both are removed simultaneously. The addition of contributions from the $\Lambda(2100)$, $\Lambda(2110)$, $\Sigma(1670)^0$ and $\Sigma(1775)^0$ states in the pK^- decay channel is also investigated. Further variations include using relativistic Breit-Wigner functions as alternative lineshapes for spin-zero $K^-\pi^+$ resonances, and altering the orbital angular-momentum-suppression factor in the Breit-Wigner formulation. Each modification to the baseline amplitude model is applied independently. The maximum absolute deviation of the fitted parameters across all alternative models, relative to the baseline result, is assigned as the corresponding systematic uncertainty.

The uncertainty associated to the background description includes the uncertainty on the background fraction f_b, estimated using an alternative model for the $m(pK^-\pi^+)$ mass shape, and that on the Legendre-polynomial parametrization, estimated varying both the background sample employed for its determination and the factorization of phase-space variables. The uncertainties related to decay kinematics and PID corrections applied to the simulation

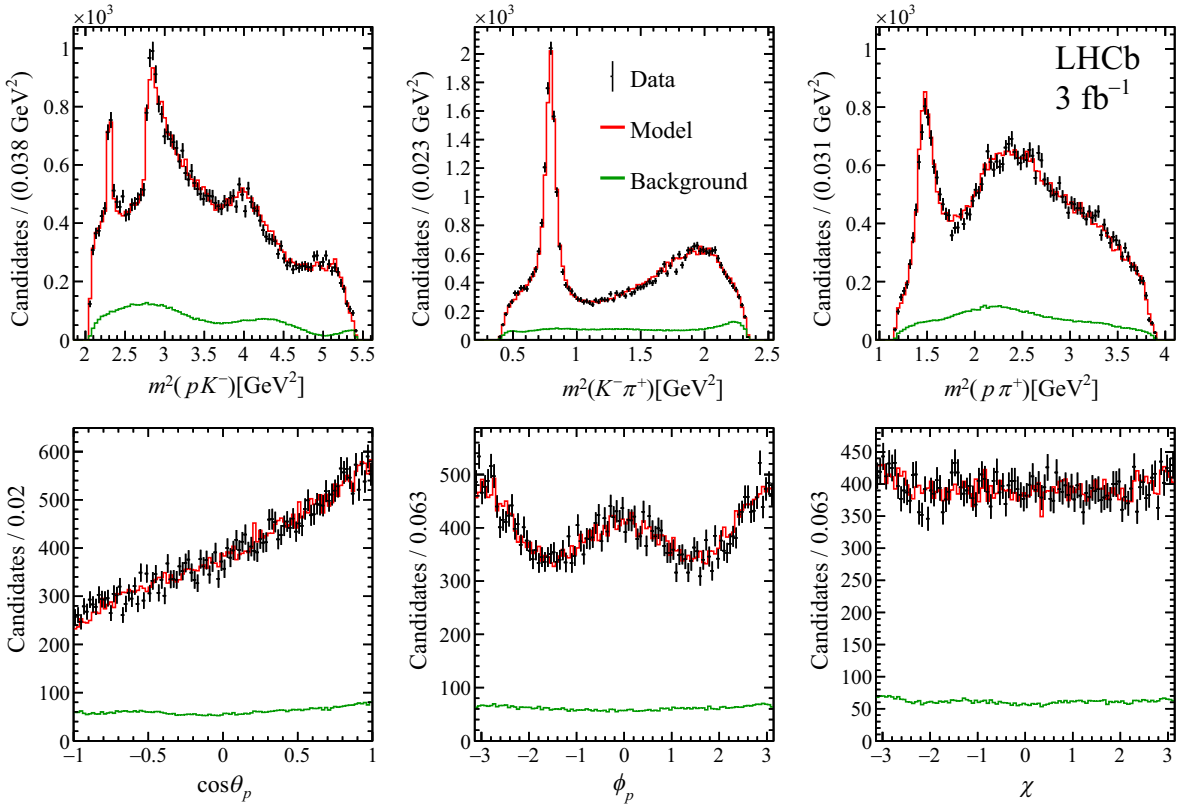

FIG. 3. Distributions for selected candidates in Run 1 together with amplitude fit projections in the $\tilde{B}$ system for (top row) invariant-mass-squared projections; and (bottom row) decay-orientation angle projections.

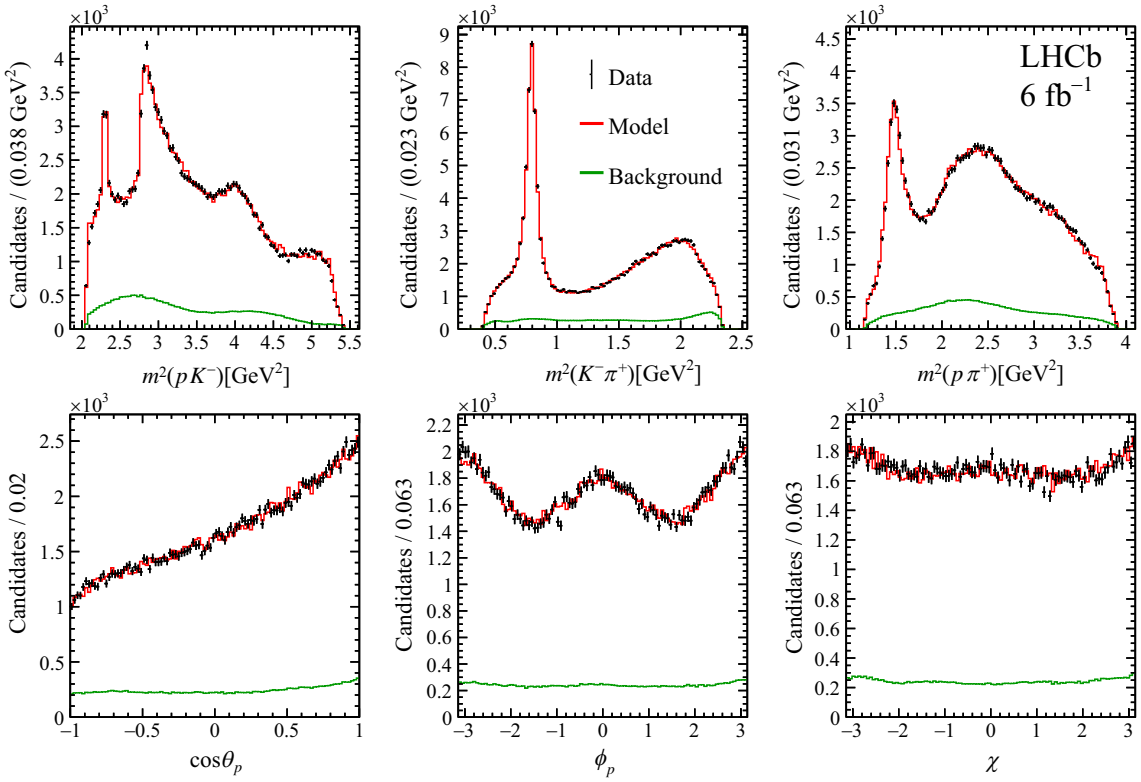

FIG. 4. Distributions for selected candidates in Run 2 together with amplitude fit projections in the $\tilde{B}$ system for (top row) invariant-mass-squared projections; and (bottom row) decay-orientation angle projections.

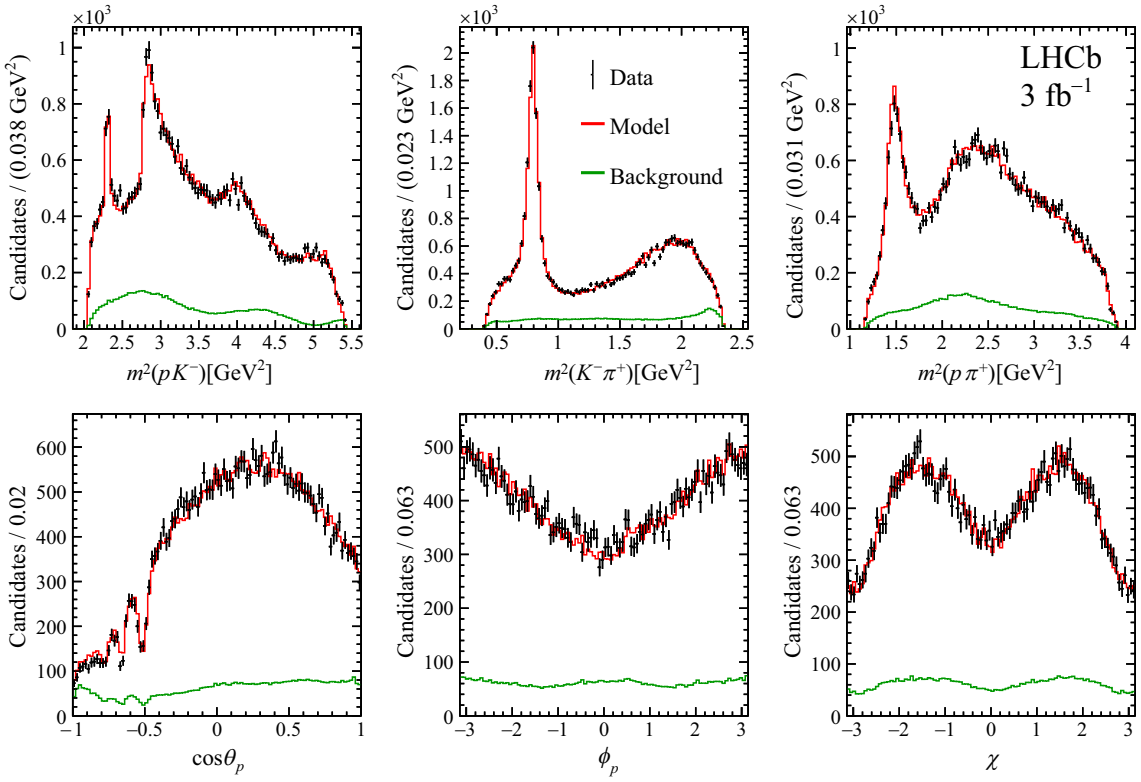

FIG. 5. Distributions for selected candidates in Run 1 together with polarization fit projections in the *lab* system for (top row) invariant-mass-squared projections; and (bottom row) decay-orientation angle projections.

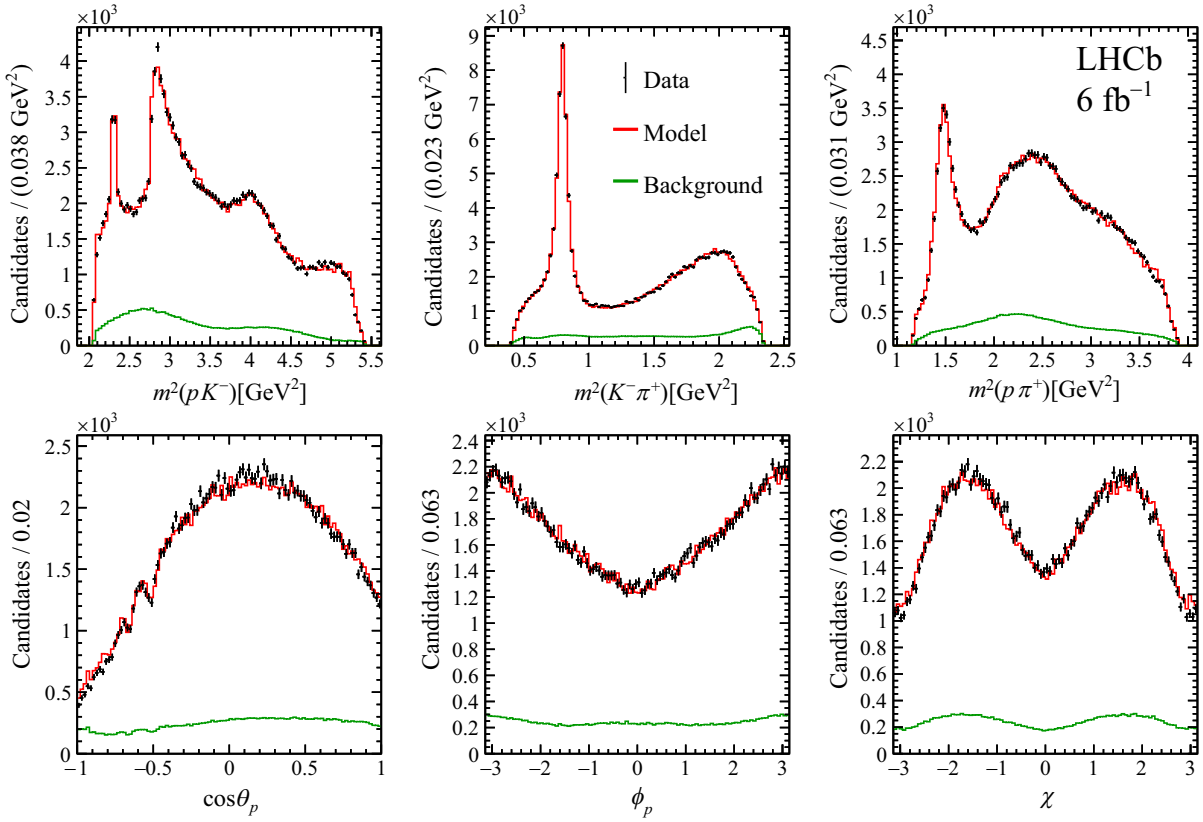

FIG. 6. Distributions for selected candidates in Run 2 together with polarization fit projections in the *lab* system for (top row) invariant-mass-squared projections; and (bottom row) decay-orientation angle projections.

are estimated separately varying the calibration samples employed and the functional form of the corrections. For the correction related to the removal of charm-meson decays in the *lab* polarization fit, a different amplitude model is employed. A possible bias in the determination of fit parameters is considered by assigning the mean deviation of 1000 pseudoexperiments from the baseline results as a systematic uncertainty. Systematic uncertainties separated for each contribution are reported in Table II for polarization components, and in the Appendix for fit parameters, fit fractions and decay asymmetries. It is worth noting that the model uncertainty on polarization components is small compared to that associated to amplitude model parameters.

The stability of the baseline amplitude model is checked by repeating the fit splitting the data set for different Ξ_c^+ charges, different data-taking periods and measuring the Ξ_c^+ polarization in the *lab* polarization system. All amplitude models obtained are compatible with the baseline within uncertainties.

VI. RESULTS

The comparison between $\Xi_c^+ \to pK^-\pi^+$ data and the baseline amplitude fit projections is displayed in Figs. 3 and 4, for Run 1 and Run 2 datasets, respectively. The comparison between $\Xi_c^+ \to pK^-\pi^+$ data and *lab*-system polarization fit projections is shown in Figs. 5 and 6. The amplitude-model distributions are obtained from the $\Xi_c^+ \to pK^-\pi^+$ simulation sample which reproduces detector efficiency effects.

The polarization components in the $\tilde{B}$ and *lab* systems are reported in Table III. The full Ξ_c^+ polarization vector is measured for the first time, with absolute uncertainties of order 1% on each component. A large polarization is measured in both Ξ_c^+ helicity frames considered. In the

TABLE III. Measured Ξ_c^+ polarization components and magnitude in $\tilde{B}$ and *lab* frames.

Component	Central value (%)	Stat. unc.	Model unc.	Syst. unc.
P_x $(\tilde{B})$	21.8	0.7	1.1	0.8
P_y $(\tilde{B})$	−0.73	0.69	0.23	0.35
P_z $(\tilde{B})$	−61.9	0.8	2.8	1.5
P $(\tilde{B})$	65.6	0.8	3.0	1.6
P_x (*lab*)	56.9	0.7	2.6	1.0
P_y (*lab*)	−0.41	0.68	0.19	0.23
P_z (*lab*)	−26.2	0.7	1.4	2.0
P (*lab*)	62.6	0.7	3.0	1.2

TABLE IV. Baseline amplitude-model measured fit parameters of the Λ contributions with lower mass.

Parameter	Central value	Statistical uncertainty	Model uncertainty	Systematic uncertainty
$\mathcal{R}e\ \mathcal{H}^{\Lambda(1405)}_{1/2,0}$	−0.74	0.22	0.69	0.17
$\mathcal{I}m\ \mathcal{H}^{\Lambda(1405)}_{1/2,0}$	0.74	0.13	0.60	0.44
$\mathcal{R}e\ \mathcal{H}^{\Lambda(1405)}_{-1/2,0}$	2.5	0.1	1.0	0.4
$\mathcal{I}m\ \mathcal{H}^{\Lambda(1405)}_{-1/2,0}$	1.1	0.2	1.5	0.6
$\mathcal{R}e\ \mathcal{H}^{\Lambda(1520)}_{1/2,0}$	−0.139	0.022	0.059	0.052
$\mathcal{I}m\ \mathcal{H}^{\Lambda(1520)}_{1/2,0}$	−0.182	0.025	0.025	0.030
$\mathcal{R}e\ \mathcal{H}^{\Lambda(1520)}_{-1/2,0}$	−0.12	0.04	0.13	0.15
$\mathcal{I}m\ \mathcal{H}^{\Lambda(1520)}_{-1/2,0}$	0.620	0.021	0.065	0.020
$\mathcal{R}e\ \mathcal{H}^{\Lambda(1600)}_{1/2,0}$	1.20	0.12	0.52	0.25
$\mathcal{I}m\ \mathcal{H}^{\Lambda(1600)}_{1/2,0}$	0.03	0.12	0.62	0.30
$\mathcal{R}e\ \mathcal{H}^{\Lambda(1600)}_{-1/2,0}$	0.51	0.13	0.73	0.64
$\mathcal{I}m\ \mathcal{H}^{\Lambda(1600)}_{-1/2,0}$	1.16	0.12	0.90	0.17
$\mathcal{R}e\ \mathcal{H}^{\Lambda(1670)}_{1/2,0}$	−0.121	0.021	0.044	0.041
$\mathcal{I}m\ \mathcal{H}^{\Lambda(1670)}_{1/2,0}$	−0.020	0.022	0.063	0.017
$\mathcal{R}e\ \mathcal{H}^{\Lambda(1670)}_{-1/2,0}$	−0.261	0.017	0.029	0.016
$\mathcal{I}m\ \mathcal{H}^{\Lambda(1670)}_{-1/2,0}$	−0.076	0.025	0.085	0.013
$\mathcal{R}e\ \mathcal{H}^{\Lambda(1690)}_{1/2,0}$	0.15	0.06	0.21	0.14
$\mathcal{I}m\ \mathcal{H}^{\Lambda(1690)}_{1/2,0}$	−0.493	0.054	0.078	0.089
$\mathcal{R}e\ \mathcal{H}^{\Lambda(1690)}_{-1/2,0}$	−0.85	0.05	0.24	0.04
$\mathcal{I}m\ \mathcal{H}^{\Lambda(1690)}_{-1/2,0}$	0.52	0.06	0.19	0.11
$\mathcal{R}e\ \mathcal{H}^{\Lambda(1710)}_{1/2,0}$	0.4	0.1	1.0	0.1
$\mathcal{I}m\ \mathcal{H}^{\Lambda(1710)}_{1/2,0}$	−0.26	0.15	0.30	0.10
$\mathcal{R}e\ \mathcal{H}^{\Lambda(1710)}_{-1/2,0}$	1.59	0.13	0.53	0.12
$\mathcal{I}m\ \mathcal{H}^{\Lambda(1710)}_{-1/2,0}$	0.36	0.17	0.75	0.48

TABLE V. Baseline amplitude-model measured fit parameters of the Λ contributions with higher mass.

Parameter	Central value	Stat. unc.	Model unc.	Syst. unc.
$\mathcal{R}e\ \mathcal{H}^{\Lambda(1800)}_{1/2,0}$	0.19	0.13	0.62	0.12
$\mathcal{I}m\ \mathcal{H}^{\Lambda(1800)}_{1/2,0}$	−0.73	0.12	0.46	0.20
$\mathcal{R}e\ \mathcal{H}^{\Lambda(1800)}_{-1/2,0}$	−0.81	0.12	0.62	0.14
$\mathcal{I}m\ \mathcal{H}^{\Lambda(1800)}_{-1/2,0}$	−0.96	0.13	0.65	0.23
$\mathcal{R}e\ \mathcal{H}^{\Lambda(1810)}_{1/2,0}$	0.05	0.10	0.36	0.07
$\mathcal{I}m\ \mathcal{H}^{\Lambda(1810)}_{1/2,0}$	0.97	0.09	0.40	0.06
$\mathcal{R}e\ \mathcal{H}^{\Lambda(1810)}_{-1/2,0}$	−0.08	0.08	0.21	0.08
$\mathcal{I}m\ \mathcal{H}^{\Lambda(1810)}_{-1/2,0}$	0.11	0.08	0.15	0.09
$\mathcal{R}e\ \mathcal{H}^{\Lambda(1820)}_{1/2,0}$	0.21	0.08	0.32	0.04
$\mathcal{I}m\ \mathcal{H}^{\Lambda(1820)}_{1/2,0}$	1.05	0.07	0.18	0.08
$\mathcal{R}e\ \mathcal{H}^{\Lambda(1820)}_{-1/2,0}$	−0.50	0.06	0.17	0.14
$\mathcal{I}m\ \mathcal{H}^{\Lambda(1820)}_{-1/2,0}$	0.04	0.06	0.21	0.18
$\mathcal{R}e\ \mathcal{H}^{\Lambda(1830)}_{1/2,0}$	0.50	0.07	0.56	0.08
$\mathcal{I}m\ \mathcal{H}^{\Lambda(1830)}_{1/2,0}$	−0.04	0.07	0.60	0.09
$\mathcal{R}e\ \mathcal{H}^{\Lambda(1830)}_{-1/2,0}$	−0.21	0.07	0.27	0.10
$\mathcal{I}m\ \mathcal{H}^{\Lambda(1830)}_{-1/2,0}$	−0.30	0.07	0.26	0.10
$\mathcal{R}e\ \mathcal{H}^{\Lambda(1890)}_{1/2,0}$	0.32	0.07	0.36	0.06
$\mathcal{I}m\ \mathcal{H}^{\Lambda(1890)}_{1/2,0}$	−0.19	0.07	0.19	0.07
$\mathcal{R}e\ \mathcal{H}^{\Lambda(1890)}_{-1/2,0}$	0.07	0.07	0.14	0.05
$\mathcal{I}m\ \mathcal{H}^{\Lambda(1890)}_{-1/2,0}$	−0.45	0.06	0.53	0.07
$\mathcal{R}e\ \mathcal{H}^{\Lambda(2000)}_{1/2,0}$	−1.45	0.14	0.36	0.17
$\mathcal{I}m\ \mathcal{H}^{\Lambda(2000)}_{1/2,0}$	−2.64	0.14	0.79	0.28
$\mathcal{R}e\ \mathcal{H}^{\Lambda(2000)}_{-1/2,0}$	−0.71	0.12	0.29	0.07
$\mathcal{I}m\ \mathcal{H}^{\Lambda(2000)}_{-1/2,0}$	−1.52	0.10	0.50	0.08

$\tilde{B}$ system it has a magnitude $P \approx 66\%$, with a dominating negative longitudinal component $P_z \approx -62\%$ and a smaller positive transverse component $P_x \approx 22\%$. In the *lab* system it has a magnitude $P \approx 63\%$, with a dominating positive transverse component $P_x \approx 57\%$ and a smaller negative longitudinal component $P_z \approx -26\%$. The normal polarization P_y, sensitive to time-reversal violation effects and final-state interactions [25], is compatible with zero at the 1% level, for both polarization systems considered. The leading uncertainty for longitudinal and transverse polarization in both systems is systematic, while for normal polarization is statistical.

The Ξ_c^+ polarization shares the features observed for the Λ_c^+ baryon [25] except for some slight differences in the measured values. The Ξ_c^+ polarization direction is more transverse and less longitudinal than that of the Λ_c^+ one in the $\tilde{B}$ frame, more longitudinal and less transverse in the *lab* frame, with a reduced magnitude in both polarization systems. Differences between Ξ_c^+ and Λ_c^+ polarization components have limited significance, being comparable in size with the uncertainties on the polarization components.

The measured parameters of the baseline amplitude model are reported in Tables IV–VII, fit fractions for each resonant contribution in Table VIII, $\sqrt{3}S$ and two-body decay-asymmetry parameters in Table IX. The amplitude analysis is sensitive to all the parameters describing the $\Xi_c^+ \to pK^-\pi^+$ amplitude model, due to the sizeable Ξ_c^+ polarization and interference effects among different decay chains [2]. The leading uncertainties come from amplitude model choice and background contributions.

TABLE VI. Baseline amplitude-model measured fit parameters of the K^* contributions.

Parameter	Central value	Stat. unc.	Model unc.	Syst. unc.
$\mathcal{R}e\ \mathcal{H}^{\bar{K}_0^*(700)^0}_{1/2,0}$	−3.95	0.23	0.86	0.37
$\mathcal{I}m\ \mathcal{H}^{\bar{K}_0^*(700)^0}_{1/2,0}$	3.0	0.3	1.5	0.6
$\mathcal{R}e\ \mathcal{H}^{\bar{K}_0^*(700)^0}_{-1/2,0}$	−2.5	0.2	1.2	0.5
$\mathcal{I}m\ \mathcal{H}^{\bar{K}_0^*(700)^0}_{-1/2,0}$	−0.35	0.19	0.99	0.22
$\gamma^{\bar{K}_0^*(700)^0}$ [GeV^{-2}]	−0.77	0.08	0.59	0.23
$\mathcal{R}e\ \mathcal{H}^{\bar{K}^*(892)^0}_{1/2,0}$	1	(fixed)		
$\mathcal{I}m\ \mathcal{H}^{\bar{K}^*(892)^0}_{1/2,0}$	0	(fixed)		
$\mathcal{R}e\ \mathcal{H}^{\bar{K}^*(892)^0}_{1/2,-1}$	1.90	0.05	0.22	0.07
$\mathcal{I}m\ \mathcal{H}^{\bar{K}^*(892)^0}_{1/2,-1}$	0.52	0.08	0.22	0.13
$\mathcal{R}e\ \mathcal{H}^{\bar{K}^*(892)^0}_{-1/2,1}$	−1.037	0.044	0.038	0.043
$\mathcal{I}m\ \mathcal{H}^{\bar{K}^*(892)^0}_{-1/2,1}$	0.19	0.06	0.24	0.05
$\mathcal{R}e\ \mathcal{H}^{\bar{K}^*(892)^0}_{-1/2,0}$	−0.24	0.08	0.23	0.03
$\mathcal{I}m\ \mathcal{H}^{\bar{K}^*(892)^0}_{-1/2,0}$	−1.20	0.05	0.17	0.02
$\mathcal{R}e\ \mathcal{H}^{\bar{K}_0^*(1430)^0}_{1/2,0}$	1.3	0.1	1.2	0.5
$\mathcal{I}m\ \mathcal{H}^{\bar{K}_0^*(1430)^0}_{1/2,0}$	1.0	0.1	1.4	0.3
$\mathcal{R}e\ \mathcal{H}^{\bar{K}_0^*(1430)^0}_{-1/2,0}$	−1.6	0.2	3.1	0.3
$\mathcal{I}m\ \mathcal{H}^{\bar{K}_0^*(1430)^0}_{-1/2,0}$	4.2	0.2	1.2	0.8
$\gamma^{\bar{K}_0^*(1430)^0}$ [GeV^{-2}]	0.05	0.02	0.27	0.07
$\mathcal{R}e\ \mathcal{H}^{\bar{K}_2^*(1430)^0}_{1/2,0}$	−1.3	0.1	1.1	0.3
$\mathcal{I}m\ \mathcal{H}^{\bar{K}_2^*(1430)^0}_{1/2,0}$	0.31	0.11	0.59	0.29
$\mathcal{R}e\ \mathcal{H}^{\bar{K}_2^*(1430)^0}_{1/2,-1}$	−0.54	0.17	0.17	0.23
$\mathcal{I}m\ \mathcal{H}^{\bar{K}_2^*(1430)^0}_{1/2,-1}$	2.49	0.13	0.88	0.18
$\mathcal{R}e\ \mathcal{H}^{\bar{K}_2^*(1430)^0}_{-1/2,1}$	1.47	0.12	0.41	0.12
$\mathcal{I}m\ \mathcal{H}^{\bar{K}_2^*(1430)^0}_{-1/2,1}$	0.85	0.15	0.65	0.16
$\mathcal{R}e\ \mathcal{H}^{\bar{K}_2^*(1430)^0}_{-1/2,0}$	0.95	0.11	0.29	0.13
$\mathcal{I}m\ \mathcal{H}^{\bar{K}_2^*(1430)^0}_{-1/2,0}$	−0.48	0.11	0.44	0.11

The largest contributions to the amplitude model, measured from fit fractions, come from the $\bar{K}^*(892)^0$, $\Delta(1232)^{++}$ and $\bar{K}_0^*(1430)^0$ resonances. Among the Λ resonances, the largest contribution is from the $\Lambda(2000)$ state, which is well-described by the spin-$1/2^-$ Breit-Wigner lineshape determined in the $\Lambda_c^+ \to pK^-\pi^+$ analysis [25]. Differences in resonance content and fit fractions of the $\Xi_c^+ \to pK^-\pi^+$ baseline model with respect to $\Lambda_c^+ \to pK^-\pi^+$ [25] show how the underlying dynamics of the two decays is different. The higher contribution of excited Λ and K^* states in the $\Xi_c^+ \to pK^-\pi^+$ case can be qualitatively

TABLE VII. Baseline amplitude-model measured fit parameters of the Δ^{++} contributions.

Parameter	Central value	Stat. unc.	Model unc.	Syst. unc.
$\mathcal{R}e\ \mathcal{H}^{\Delta(1232)^{++}}_{1/2,0}$	−1.50	0.08	0.14	0.06
$\mathcal{I}m\ \mathcal{H}^{\Delta(1232)^{++}}_{1/2,0}$	−0.07	0.10	0.25	0.14
$\mathcal{R}e\ \mathcal{H}^{\Delta(1232)^{++}}_{-1/2,0}$	−3.32	0.16	0.32	0.05
$\mathcal{I}m\ \mathcal{H}^{\Delta(1232)^{++}}_{-1/2,0}$	2.58	0.79	0.29	0.27
$\mathcal{R}e\ \mathcal{H}^{\Delta(1600)^{++}}_{1/2,0}$	0.3	0.2	1.2	0.6
$\mathcal{I}m\ \mathcal{H}^{\Delta(1600)^{++}}_{1/2,0}$	−2.99	0.15	0.71	0.33
$\mathcal{R}e\ \mathcal{H}^{\Delta(1600)^{++}}_{-1/2,0}$	0.0	0.2	1.1	0.3
$\mathcal{I}m\ \mathcal{H}^{\Delta(1600)^{++}}_{-1/2,0}$	−2.08	0.13	0.30	0.35
$\mathcal{R}e\ \mathcal{H}^{\Delta(1620)^{++}}_{1/2,0}$	0.00	0.08	0.33	0.10
$\mathcal{I}m\ \mathcal{H}^{\Delta(1620)^{++}}_{1/2,0}$	1.20	0.05	0.40	0.05
$\mathcal{R}e\ \mathcal{H}^{\Delta(1620)^{++}}_{-1/2,0}$	−0.67	0.06	0.28	0.21
$\mathcal{I}m\ \mathcal{H}^{\Delta(1620)^{++}}_{-1/2,0}$	−0.62	0.07	0.22	0.08
$\mathcal{R}e\ \mathcal{H}^{\Delta(1700)^{++}}_{1/2,0}$	1.1	0.2	1.1	0.1
$\mathcal{I}m\ \mathcal{H}^{\Delta(1700)^{++}}_{1/2,0}$	−1.87	0.13	0.72	0.25
$\mathcal{R}e\ \mathcal{H}^{\Delta(1700)^{++}}_{-1/2,0}$	1.49	0.13	0.50	0.60
$\mathcal{I}m\ \mathcal{H}^{\Delta(1700)^{++}}_{-1/2,0}$	−1.09	0.13	0.50	0.13

TABLE VIII. Fit fractions in % of the resonant contributions included in the baseline amplitude model.

Resonance	Central value	Stat. unc.	Model unc.	Syst. unc.
$\Lambda(1405)$	3.3	0.2	1.5	0.2
$\Lambda(1520)$	2.64	0.08	0.11	0.04
$\Lambda(1600)$	2.0	0.3	1.4	1.0
$\Lambda(1670)$	3.03	0.09	0.17	0.11
$\Lambda(1690)$	1.55	0.12	0.40	0.42
$\Lambda(1710)$	2.3	0.3	1.8	0.4
$\Lambda(1800)$	1.48	0.13	0.58	0.15
$\Lambda(1810)$	1.33	0.28	0.96	0.17
$\Lambda(1820)$	0.82	0.09	0.14	0.08
$\Lambda(1830)$	0.20	0.05	0.10	0.03
$\Lambda(1890)$	0.19	0.05	0.17	0.04
$\Lambda(2000)$	7.4	0.3	1.1	0.8
$\bar{K}_0^*(700)^0$	7.4	0.4	4.8	0.7
$\bar{K}^*(892)^0$	28.61	0.28	0.82	0.80
$\bar{K}_0^*(1430)^0$	15.6	0.7	7.1	1.9
$\bar{K}_2^*(1430)^0$	3.3	0.2	2.7	0.7
$\Delta(1232)^{++}$	17.2	0.4	1.3	0.5
$\Delta(1600)^{++}$	4.31	0.27	0.96	0.91
$\Delta(1620)^{++}$	3.29	0.21	0.98	0.27
$\Delta(1700)^{++}$	2.01	0.17	0.44	0.15

TABLE IX. Sensitivity to polarization $\sqrt{3}S$ and decay-asymmetry α parameters of single resonant contributions.

Resonance	α	Stat. unc.	Model unc.	Syst. unc.
Model $\sqrt{3}S$	0.691	0.005	0.029	0.009
$\bar{K}^*(892)^0$ $\sqrt{3}S$	0.613	0.016	0.062	0.014
$\bar{K}_2^*(1430)^0$ $\sqrt{3}S$	0.36	0.05	0.15	0.08
$\Lambda(1405)$	−0.75	0.09	0.28	0.08
$\Lambda(1520)$	−0.77	0.04	0.11	0.06
$\Lambda(1600)$	−0.06	0.11	0.39	0.08
$\Lambda(1670)$	−0.66	0.06	0.13	0.11
$\Lambda(1690)$	−0.58	0.07	0.07	0.12
$\Lambda(1710)$	−0.86	0.09	0.35	0.06
$\Lambda(1800)$	−0.47	0.30	0.95	0.71
$\Lambda(1810)$	0.96	0.06	0.42	0.08
$\Lambda(1820)$	0.64	0.07	0.19	0.21
$\Lambda(1830)$	0.30	0.19	0.91	0.41
$\Lambda(1890)$	−0.19	0.19	0.51	0.21
$\Lambda(2000)$	0.53	0.04	0.13	0.05
$\bar{K}_0^*(700)^0$	0.60	0.04	0.10	0.06
$\bar{K}_0^*(1430)^0$	−0.758	0.028	0.081	0.054
$\Delta(1232)^{++}$	−0.774	0.020	0.066	0.019
$\Delta(1600)^{++}$	0.35	0.06	0.27	0.06
$\Delta(1620)^{++}$	0.26	0.06	0.31	0.22
$\Delta(1700)^{++}$	0.15	0.07	0.17	0.24

explained by the presence of a valence s quark in the Ξ_c^+ baryon, which can be directly passed to the strange resonances. In the $\Lambda_c^+ \to pK^-\pi^+$ case, the strangeness of intermediate resonances has to be produced in the Λ_c^+ weak decay.

A large sensitivity of the $\Xi_c^+ \to pK^-\pi^+$ decay to the polarization is measured, $\sqrt{3}S = 0.691 \pm 0.005 \pm 0.030$, which is also an observation of parity violation. This value is comparable with the sensitivity to Λ_c^+ polarization measured for the $\Lambda_c^+ \to pK^-\pi^+$ decay [25], $\sqrt{3}S \approx 0.662$. The large sensitivity makes the decay suitable for Ξ_c^+ polarization measurements in other systems. Many two-body decay-asymmetry parameters are significantly different from zero, indicating parity violation in these resonant decay contributions.

VII. SUMMARY

An amplitude analysis of $\Xi_c^+ \to pK^-\pi^+$ decays with a measurement of the Ξ_c^+ polarization vector in semileptonic beauty-hadron decays is presented. Candidates are selected from pp collisions recorded with the LHCb detector at center-of-mass energies of 7, 8, and 13 TeV, corresponding to an integrated luminosity of 9 fb^{-1}. All the parameters of the amplitude model and the baryon polarization have been measured; fit fractions and decay-asymmetry parameters for each two-body resonant contribution are also reported together with the effective three-body decay-asymmetry parameter of the $\Xi_c^+ \to pK^-\pi^+$ decay. The most important resonances contributing to the $\Xi_c^+ \to pK^-\pi^+$ decay are the $\bar{K}^*(892)^0$, $\Delta(1232)^{++}$, and $\bar{K}_0^*(1430)^0$ states. Among the Λ resonances the largest contribution is from the $\Lambda(2000)$ state. A large Ξ_c^+ polarization of order 63–66% is found, measured with absolute uncertainties of order 1%. The normal polarization, sensitive to time-reversal violation effects and final-state interactions, is compatible with zero. A large sensitivity to the polarization is measured, making the amplitude model suitable for Ξ_c^+ polarization measurements in other systems. The amplitude model obtained provides a complete description of the $\Xi_c^+ \to pK^-\pi^+$ decay, with applications ranging from new physics searches to low-energy QCD. Such applications include an increased sensitivity to angular analyses of semileptonic baryon decays, and measurements of the Ξ_c^+ polarization and electromagnetic dipole moments via spin precession.

ACKNOWLEDGMENTS

We express our gratitude to our colleagues in the CERN accelerator departments for the excellent performance of the LHC. We thank the technical and administrative staff at the LHCb institutes. We acknowledge support from CERN and from the national agencies: ARC (Australia); CAPES, CNPq, FAPERJ and FINEP (Brazil); MOST and NSFC (China); CNRS/IN2P3 (France); BMBF, DFG and MPG (Germany); INFN (Italy); NWO (Netherlands); MNiSW and NCN (Poland); MCID/IFA (Romania); MICIU and AEI (Spain); SNSF and SER (Switzerland); NASU (Ukraine); STFC (United Kingdom); DOE NP and NSF (USA). We acknowledge the computing resources that are provided by ARDC (Australia), CBPF (Brazil), CERN, IHEP and LZU (China), IN2P3 (France), KIT and DESY (Germany), INFN (Italy), SURF (Netherlands), Polish WLCG (Poland), IFIN-HH (Romania), PIC (Spain), CSCS (Switzerland), and GridPP (United Kingdom). We are indebted to the communities behind the multiple open-source software packages on which we depend. Individual groups or members have received support from Key Research Program of Frontier Sciences of CAS, CAS PIFI, CAS CCEPP, Fundamental Research Funds for the Central Universities, and Sci. & Tech. Program of Guangzhou (China); Minciencias (Colombia); EPLANET, Marie Skłodowska-Curie Actions, ERC and NextGenerationEU (European Union); A*MIDEX, ANR, IPhU and Labex P2IO, and Région Auvergne-Rhône-Alpes (France); Alexander-von-Humboldt Foundation (Germany); ICSC (Italy); Severo Ochoa and María de Maeztu Units of Excellence, GVA, XuntaGal, GENCAT, InTalent-Inditex and Prog. Atracción Talento CM (Spain); SRC (Sweden); the Leverhulme Trust, the Royal Society and UKRI (United Kingdom).

DATA AVAILABILITY

The data that support the findings of this article are openly available [53].

APPENDIX: SUMMARY OF SYSTEMATIC UNCERTAINTY CONTRIBUTIONS

Systematic uncertainties separated for each contribution are reported in Tables X–XIII for fit parameters, Table XIV for fit fractions, and Table XV for decay asymmetries.

TABLE X. Systematic uncertainty contributions on fit parameters describing the Λ contributions with lower mass. Total* includes all contributions except for the choice of amplitude model.

Parameter	Model	Total*	Background	Kinematics	PID	Fit bias
$\mathcal{R}e\ \mathcal{H}^{\Lambda(1405)}_{1/2,0}$	0.69	0.17	0.17	<0.01	0.02	<0.01
$\mathcal{I}m\ \mathcal{H}^{\Lambda(1405)}_{1/2,0}$	0.60	0.44	0.41	0.15	0.01	0.01
$\mathcal{R}e\ \mathcal{H}^{\Lambda(1405)}_{-1/2,0}$	1.0	0.4	0.4	<0.1	<0.1	<0.1
$\mathcal{I}m\ \mathcal{H}^{\Lambda(1405)}_{-1/2,0}$	1.5	0.6	0.6	<0.1	<0.1	<0.1
$\mathcal{R}e\ \mathcal{H}^{\Lambda(1520)}_{1/2,0}$	0.059	0.052	0.051	0.003	0.009	0.002
$\mathcal{I}m\ \mathcal{H}^{\Lambda(1520)}_{1/2,0}$	0.025	0.030	0.022	0.021	0.004	0.001
$\mathcal{R}e\ \mathcal{H}^{\Lambda(1520)}_{-1/2,0}$	0.13	0.15	0.15	<0.01	0.01	<0.01
$\mathcal{I}m\ \mathcal{H}^{\Lambda(1520)}_{-1/2,0}$	0.065	0.020	0.019	0.007	0.002	0.001
$\mathcal{R}e\ \mathcal{H}^{\Lambda(1600)}_{1/2,0}$	0.52	0.25	0.24	0.05	0.02	0.01
$\mathcal{I}m\ \mathcal{H}^{\Lambda(1600)}_{1/2,0}$	0.62	0.30	0.29	0.01	0.06	0.01
$\mathcal{R}e\ \mathcal{H}^{\Lambda(1600)}_{-1/2,0}$	0.73	0.64	0.64	0.04	0.03	<0.01
$\mathcal{I}m\ \mathcal{H}^{\Lambda(1600)}_{-1/2,0}$	0.90	0.17	0.17	0.03	0.02	0.01
$\mathcal{R}e\ \mathcal{H}^{\Lambda(1670)}_{1/2,0}$	0.044	0.041	0.039	0.010	0.007	0.002
$\mathcal{I}m\ \mathcal{H}^{\Lambda(1670)}_{1/2,0}$	0.063	0.017	0.017	<0.001	0.003	<0.001
$\mathcal{R}e\ \mathcal{H}^{\Lambda(1670)}_{-1/2,0}$	0.029	0.016	0.012	0.007	0.008	<0.001
$\mathcal{I}m\ \mathcal{H}^{\Lambda(1670)}_{-1/2,0}$	0.085	0.013	0.009	0.008	0.006	0.001
$\mathcal{R}e\ \mathcal{H}^{\Lambda(1690)}_{1/2,0}$	0.21	0.14	0.13	0.03	0.01	<0.01
$\mathcal{I}m\ \mathcal{H}^{\Lambda(1690)}_{1/2,0}$	0.079	0.089	0.084	0.030	0.004	0.001
$\mathcal{R}e\ \mathcal{H}^{\Lambda(1690)}_{-1/2,0}$	0.24	0.04	0.04	<0.01	0.01	<0.01
$\mathcal{I}m\ \mathcal{H}^{\Lambda(1690)}_{-1/2,0}$	0.19	0.11	0.11	0.01	0.01	<0.01
$\mathcal{R}e\ \mathcal{H}^{\Lambda(1710)}_{1/2,0}$	1.0	0.1	0.1	0.1	0.1	<0.1
$\mathcal{I}m\ \mathcal{H}^{\Lambda(1710)}_{1/2,0}$	0.30	0.10	0.09	0.03	0.02	<0.01
$\mathcal{R}e\ \mathcal{H}^{\Lambda(1710)}_{-1/2,0}$	0.53	0.12	0.12	0.03	0.02	0.01
$\mathcal{I}m\ \mathcal{H}^{\Lambda(1710)}_{-1/2,0}$	0.75	0.48	0.48	0.02	0.04	<0.01

TABLE XI. Systematic uncertainty contributions on fit parameters describing the Λ contributions with higher mass. Total* includes all contributions except for the choice of amplitude model.

Parameter	Model	Total*	Background	Kinematics	PID	Fit bias
$\mathcal{R}e\ \mathcal{H}^{\Lambda(1800)}_{1/2,0}$	0.62	0.12	0.11	0.04	0.01	<0.01
$\mathcal{I}m\ \mathcal{H}^{\Lambda(1800)}_{1/2,0}$	0.46	0.20	0.19	0.07	0.01	0.01
$\mathcal{R}e\ \mathcal{H}^{\Lambda(1800)}_{-1/2,0}$	0.62	0.14	0.14	0.02	0.01	0.01
$\mathcal{I}m\ \mathcal{H}^{\Lambda(1800)}_{-1/2,0}$	0.65	0.23	0.23	0.01	0.01	<0.01
$\mathcal{R}e\ \mathcal{H}^{\Lambda(1810)}_{1/2,0}$	0.36	0.07	0.06	0.03	0.01	<0.01
$\mathcal{I}m\ \mathcal{H}^{\Lambda(1810)}_{1/2,0}$	0.40	0.06	0.05	<0.01	0.02	<0.01
$\mathcal{R}e\ \mathcal{H}^{\Lambda(1810)}_{-1/2,0}$	0.21	0.08	0.07	0.04	0.01	<0.01
$\mathcal{I}m\ \mathcal{H}^{\Lambda(1810)}_{-1/2,0}$	0.20	0.09	0.08	0.02	0.02	<0.01
$\mathcal{R}e\ \mathcal{H}^{\Lambda(1820)}_{1/2,0}$	0.32	0.04	0.04	0.01	0.01	<0.01
$\mathcal{I}m\ \mathcal{H}^{\Lambda(1820)}_{1/2,0}$	0.18	0.08	0.07	<0.01	0.02	<0.00
$\mathcal{R}e\ \mathcal{H}^{\Lambda(1820)}_{-1/2,0}$	0.17	0.14	0.13	0.02	<0.01	<0.01
$\mathcal{I}m\ \mathcal{H}^{\Lambda(1820)}_{-1/2,0}$	0.21	0.18	0.18	0.01	0.01	<0.01
$\mathcal{R}e\ \mathcal{H}^{\Lambda(1830)}_{1/2,0}$	0.56	0.08	0.07	0.01	0.01	<0.01
$\mathcal{I}m\ \mathcal{H}^{\Lambda(1830)}_{1/2,0}$	0.59	0.09	0.09	<0.01	0.01	<0.01
$\mathcal{R}e\ \mathcal{H}^{\Lambda(1830)}_{-1/2,0}$	0.27	0.10	0.09	0.02	0.04	<0.01
$\mathcal{I}m\ \mathcal{H}^{\Lambda(1830)}_{-1/2,0}$	0.26	0.10	0.09	0.03	0.03	<0.01
$\mathcal{R}e\ \mathcal{H}^{\Lambda(1890)}_{1/2,0}$	0.36	0.06	0.05	0.02	0.01	<0.01
$\mathcal{I}m\ \mathcal{H}^{\Lambda(1890)}_{1/2,0}$	0.19	0.08	0.07	0.02	0.01	0.01
$\mathcal{R}e\ \mathcal{H}^{\Lambda(1890)}_{-1/2,0}$	0.14	0.05	0.05	<0.01	0.02	<0.01
$\mathcal{I}m\ \mathcal{H}^{\Lambda(1890)}_{-1/2,0}$	0.53	0.07	0.07	<0.01	0.01	<0.01
$\mathcal{R}e\ \mathcal{H}^{\Lambda(2000)}_{1/2,0}$	0.36	0.17	0.11	0.12	0.02	<0.01
$\mathcal{I}m\ \mathcal{H}^{\Lambda(2000)}_{1/2,0}$	0.79	0.28	0.27	0.02	0.03	<0.01
$\mathcal{R}e\ \mathcal{H}^{\Lambda(2000)}_{-1/2,0}$	0.29	0.07	0.07	0.02	0.01	0.01
$\mathcal{I}m\ \mathcal{H}^{\Lambda(2000)}_{-1/2,0}$	0.50	0.08	0.07	0.02	0.02	<0.01

TABLE XII. Systematic uncertainty contributions on fit parameters describing K^* contributions. Total* includes all contributions except for the choice of amplitude model.

Parameter	Model	Total*	Background	Kinematics	PID	Fit bias
$\mathcal{R}e\ \mathcal{H}^{\bar{K}_0^*(700)^0}_{1/2,0}$	0.86	0.37	0.36	0.08	0.07	0.02
$\mathcal{I}m\ \mathcal{H}^{\bar{K}_0^*(700)^0}_{1/2,0}$	1.5	0.6	0.5	0.2	0.1	<0.1
$\mathcal{R}e\ \mathcal{H}^{\bar{K}_0^*(700)^0}_{-1/2,0}$	1.2	0.5	0.5	<0.1	0.1	0.1
$\mathcal{I}m\ \mathcal{H}^{\bar{K}_0^*(700)^0}_{-1/2,0}$	0.99	0.22	0.21	0.02	0.04	0.01
$\gamma^{\bar{K}_0^*(700)^0}$ [GeV^{-2}]	0.59	0.23	0.23	0.01	0.03	<0.01
$\mathcal{R}e\ \mathcal{H}^{\bar{K}^*(892)^0}_{1/2,0}$			0 (fixed)			
$\mathcal{I}m\ \mathcal{H}^{\bar{K}^*(892)^0}_{1/2,0}$			0 (fixed)			
$\mathcal{R}e\ \mathcal{H}^{\bar{K}^*(892)^0}_{1/2,-1}$	0.22	0.08	0.06	0.03	0.02	0.01
$\mathcal{I}m\ \mathcal{H}^{\bar{K}^*(892)^0}_{1/2,-1}$	0.22	0.13	0.12	0.03	0.01	0.01
$\mathcal{R}e\ \mathcal{H}^{\bar{K}^*(892)^0}_{-1/2,1}$	0.038	0.043	0.043	0.001	0.003	0.003
$\mathcal{I}m\ \mathcal{H}^{\bar{K}^*(892)^0}_{-1/2,1}$	0.24	0.05	0.04	0.03	0.01	<0.01
$\mathcal{R}e\ \mathcal{H}^{\bar{K}^*(892)^0}_{-1/2,0}$	0.23	0.03	0.02	0.02	0.01	<0.01
$\mathcal{I}m\ \mathcal{H}^{\bar{K}^*(892)^0}_{-1/2,0}$	0.17	0.02	0.02	0.01	0.01	0.01
$\mathcal{R}e\ \mathcal{H}^{\bar{K}_0^*(1430)^0}_{1/2,0}$	1.2	0.5	0.5	0.1	0.1	<0.1
$\mathcal{I}m\ \mathcal{H}^{\bar{K}_0^*(1430)^0}_{1/2,0}$	1.4	0.3	0.3	<0.1	<0.1	<0.1
$\mathcal{R}e\ \mathcal{H}^{\bar{K}_0^*(1430)^0}_{-1/2,0}$	3.1	0.3	0.3	0.1	<0.1	<0.1
$\mathcal{I}m\ \mathcal{H}^{\bar{K}_0^*(1430)^0}_{-1/2,0}$	1.2	0.8	0.8	0.1	0.1	0.1
$\gamma^{\bar{K}_0^*(1430)^0}$ [GeV^{-2}]	0.27	0.07	0.07	<0.01	<0.01	<0.01
$\mathcal{R}e\ \mathcal{H}^{\bar{K}_2^*(1430)^0}_{1/2,0}$	1.1	0.3	0.3	<0.1	<0.1	<0.1
$\mathcal{I}m\ \mathcal{H}^{\bar{K}_2^*(1430)^0}_{1/2,0}$	0.59	0.29	0.29	0.04	0.01	0.01
$\mathcal{R}e\ \mathcal{H}^{\bar{K}_2^*(1430)^0}_{1/2,-1}$	0.17	0.23	0.20	0.11	0.03	<0.01
$\mathcal{I}m\ \mathcal{H}^{\bar{K}_2^*(1430)^0}_{1/2,-1}$	0.88	0.18	0.16	0.07	0.01	0.01
$\mathcal{R}e\ \mathcal{H}^{\bar{K}_2^*(1430)^0}_{-1/2,1}$	0.41	0.12	0.08	0.07	0.05	<0.01
$\mathcal{I}m\ \mathcal{H}^{\bar{K}_2^*(1430)^0}_{-1/2,1}$	0.65	0.16	0.15	0.03	0.03	<0.01
$\mathcal{R}e\ \mathcal{H}^{\bar{K}_2^*(1430)^0}_{-1/2,0}$	0.29	0.13	0.12	0.06	0.03	<0.01
$\mathcal{I}m\ \mathcal{H}^{\bar{K}_2^*(1430)^0}_{-1/2,0}$	0.44	0.11	0.10	0.03	0.03	<0.01

TABLE XIII. Systematic uncertainty contributions on fit parameters describing Δ^{++} contributions. Total* includes all contributions except for the choice of amplitude model.

Parameter	Model	Total*	Background	Kinematics	PID	Fit bias
$\mathcal{R}e\ \mathcal{H}^{\Delta(1232)^{++}}_{1/2,0}$	0.14	0.06	0.05	<0.01	0.02	<0.01
$\mathcal{I}m\ \mathcal{H}^{\Delta(1232)^{++}}_{1/2,0}$	0.25	0.14	0.13	0.05	0.02	<0.01
$\mathcal{R}e\ \mathcal{H}^{\Delta(1232)^{++}}_{-1/2,0}$	0.32	0.05	0.05	0.01	0.02	0.01
$\mathcal{I}m\ \mathcal{H}^{\Delta(1232)^{++}}_{-1/2,0}$	0.79	0.27	0.26	0.07	0.06	0.01
$\mathcal{R}e\ \mathcal{H}^{\Delta(1600)^{++}}_{1/2,0}$	1.2	0.6	0.6	<0.1	<0.1	<0.1
$\mathcal{I}m\ \mathcal{H}^{\Delta(1600)^{++}}_{1/2,0}$	0.71	0.33	0.33	0.03	0.05	<0.01
$\mathcal{R}e\ \mathcal{H}^{\Delta(1600)^{++}}_{-1/2,0}$	1.1	0.3	0.2	<0.1	<0.1	<0.1
$\mathcal{I}m\ \mathcal{H}^{\Delta(1600)^{++}}_{-1/2,0}$	0.30	0.35	0.34	0.05	0.03	<0.01
$\mathcal{R}e\ \mathcal{H}^{\Delta(1620)^{++}}_{1/2,0}$	0.33	0.10	0.10	<0.01	0.02	<0.01
$\mathcal{I}m\ \mathcal{H}^{\Delta(1620)^{++}}_{1/2,0}$	0.40	0.05	0.05	0.01	0.01	<0.01
$\mathcal{R}e\ \mathcal{H}^{\Delta(1620)^{++}}_{-1/2,0}$	0.28	0.21	0.21	0.04	0.01	<0.01
$\mathcal{I}m\ \mathcal{H}^{\Delta(1620)^{++}}_{-1/2,0}$	0.22	0.08	0.08	0.01	<0.01	<0.01
$\mathcal{R}e\ \mathcal{H}^{\Delta(1700)^{++}}_{1/2,0}$	1.1	0.1	0.1	<0.1	0.1	<0.1
$\mathcal{I}m\ \mathcal{H}^{\Delta(1700)^{++}}_{1/2,0}$	0.72	0.25	0.23	0.03	0.09	<0.01
$\mathcal{R}e\ \mathcal{H}^{\Delta(1700)^{++}}_{-1/2,0}$	0.50	0.60	0.59	0.04	0.08	0.01
$\mathcal{I}m\ \mathcal{H}^{\Delta(1700)^{++}}_{-1/2,0}$	0.50	0.13	0.10	0.06	0.04	<0.01

TABLE XIV. Systematic uncertainty contributions on fit fractions. Total* includes all contributions except for the choice of the amplitude model.

Resonance	Model	Total*	Background	Kinematics	PID	Fit bias
$\Lambda(1405)$	0.015	0.002	0.002	<0.001	<0.001	<0.001
$\Lambda(1520)$	0.0011	0.0004	0.0004	0.0001	<0.0001	0.0001
$\Lambda(1600)$	0.014	0.010	0.010	0.001	0.001	<0.001
$\Lambda(1670)$	0.0017	0.0011	0.0011	<0.0001	0.0001	0.0002
$\Lambda(1690)$	0.0040	0.0042	0.0042	<0.0001	<0.0001	<0.0001
$\Lambda(1710)$	0.018	0.004	0.004	<0.001	0.001	0.001
$\Lambda(1800)$	0.0058	0.0015	0.0014	0.0003	0.0001	0.0004
$\Lambda(1810)$	0.0096	0.0017	0.0012	0.0004	0.0011	0.0002
$\Lambda(1820)$	0.0014	0.0008	0.0008	0.0001	0.0002	<0.0001
$\Lambda(1830)$	0.0010	0.0003	0.0003	0.0001	0.0001	0.0001
$\Lambda(1890)$	0.0017	0.0004	0.0004	0.0001	0.0001	0.0001
$\Lambda(2000)$	0.011	0.008	0.008	0.001	0.001	<0.001
$\bar{K}^*_0(700)^0$	0.048	0.007	0.006	<0.001	0.002	<0.001
$\bar{K}^*(892)^0$	0.0082	0.0080	0.0076	0.0024	0.0005	0.0005
$\bar{K}^*_0(1430)^0$	0.071	0.019	0.018	0.003	0.004	<0.001
$\bar{K}^*_2(1430)^0$	0.027	0.007	0.006	0.002	0.001	<0.001
$\Delta(1232)^{++}$	0.013	0.005	0.004	0.002	0.001	<0.001
$\Delta(1600)^{++}$	0.0096	0.0091	0.0091	0.0001	0.0006	0.0002
$\Delta(1620)^{++}$	0.0098	0.0027	0.0027	0.0003	0.0003	<0.0001
$\Delta(1700)^{++}$	0.0044	0.0015	0.0012	0.0003	0.0008	0.0003

TABLE XV. Systematic uncertainties on $\sqrt{3}S$ and decay-asymmetry parameters. Total* includes all contributions except for the choice of amplitude model.

α	Model	Total*	Background	Kinematics	PID	Fit bias
Model $\sqrt{3}S$	0.029	0.009	0.008	0.001	0.003	<0.001
$\bar{K}^*(892)^0$ $\sqrt{3}S$	0.062	0.014	0.009	0.009	0.006	0.001
$\bar{K}_2^*(1430)^0$ $\sqrt{3}S$	0.15	0.08	0.07	<0.01	0.02	<0.01
$\Lambda(1405)$	0.28	0.08	0.05	0.05	0.02	0.01
$\Lambda(1520)$	0.11	0.06	0.04	0.04	0.01	<0.01
$\Lambda(1600)$	0.39	0.08	0.07	0.03	0.01	<0.01
$\Lambda(1670)$	0.13	0.11	0.10	0.03	0.03	0.01
$\Lambda(1690)$	0.07	0.12	0.12	0.01	0.01	<0.01
$\Lambda(1710)$	0.35	0.06	0.05	0.03	0.02	0.02
$\Lambda(1800)$	0.95	0.71	0.68	0.19	0.03	0.02
$\Lambda(1810)$	0.43	0.08	0.07	0.03	0.01	0.02
$\Lambda(1820)$	0.19	0.21	0.21	0.02	0.01	0.01
$\Lambda(1830)$	0.91	0.41	0.41	<0.01	0.02	<0.01
$\Lambda(1890)$	0.51	0.21	0.20	0.04	0.04	0.01
$\Lambda(2000)$	0.13	0.05	0.05	<0.01	0.01	<0.01
$\bar{K}_0^*(700)^0$	0.10	0.06	0.05	<0.01	0.02	<0.01
$\bar{K}_0^*(1430)^0$	0.081	0.054	0.054	0.010	0.003	<0.001
$\Delta(1232)^{++}$	0.066	0.019	0.017	0.004	0.007	0.001
$\Delta(1600)^{++}$	0.27	0.06	0.05	0.03	0.01	<0.01
$\Delta(1620)^{++}$	0.31	0.22	0.21	0.02	0.01	<0.01
$\Delta(1700)^{++}$	0.17	0.24	0.24	<0.01	0.03	<0.01

[1] S. Navas *et al.* (Particle Data Group), Review of particle physics, Phys. Rev. D **110**, 030001 (2024).

[2] D. Marangotto, Extracting maximum information from polarised baryon decays via amplitude analysis: The $\Lambda_c^+ \to pK^-\pi^+$ case, Adv. High Energy Phys. **2020**, 7463073 (2020).

[3] R. Aaij *et al.* (LHCb Collaboration), Observation of the decay $\Lambda_b^0 \to pK^-\mu^+\mu^-$ and search for *CP* violation, J. High Energy Phys. 06 (2017) 108.

[4] R. Aaij *et al.* (LHCb Collaboration), Search for *CP* violation in $\Lambda_c^+ \to pK^-K^+$ and $\Lambda_c^+ \to p\pi^-\pi^+$ decays, J. High Energy Phys. 03 (2018) 182.

[5] R. Aaij *et al.* (LHCb Collaboration), Search for *CP* violation using triple product asymmetries in $\Lambda_b^0 \to pK^-\pi^+\pi^-$, $\Lambda_b^0 \to pK^-K^+K^-$, and $\Xi_b^0 \to pK^-K^-\pi^+$ decays, J. High Energy Phys. 08 (2018) 039.

[6] R. Aaij *et al.* (LHCb Collaboration), Search for *CP* violation in $\Lambda_b^0 \to pK^-$ and $\Lambda_b^0 \to p\pi^-$ decays, Phys. Lett. B **784**, 101 (2018).

[7] R. Aaij *et al.* (LHCb Collaboration), Measurement of *CP* asymmetries in charmless four-body Λ_b^0 and Ξ_b^0 decays, Eur. Phys. J. C **79**, 745 (2019).

[8] R. Aaij *et al.* (LHCb Collaboration), Search for *CP* violation in $\Xi_c^+ \to pK^-\pi^+$ decays with model-independent techniques, Eur. Phys. J. C **80**, 986 (2020).

[9] R. Aaij *et al.* (LHCb Collaboration), Search for *CP* violation and observation of *P* violation in $\Lambda_b^0 \to p\pi^-\pi^+\pi^-$ decays, Phys. Rev. D **102**, 051101 (2020).

[10] R. Aaij *et al.* (LHCb Collaboration), Study of Λ_b^0 and Ξ_b^0 decays to $\Lambda h^+h'^-$ and evidence for *CP* violation in $\Lambda_b^0 \to \Lambda K^+K^-$, Phys. Rev. Lett. **134**, 101802 (2025).

[11] M. Davier, L. Duflot, F. Le Diberder, and A. Rouge, The optimal method for the measurement of tau polarization, Phys. Lett. B **306**, 411 (1993).

[12] J. Zhang, X. An, R. Sun, and J. Su, Probing new physics in semileptonic $\Xi_b \to \Lambda(\Xi_c)\tau^-\bar{\nu}_\tau$ decays, Eur. Phys. J. C **79**, 863 (2019).

[13] S.-W. Wang, $\Xi_b \to \Xi_c\tau\bar{\nu}_\tau$ decay in new physics models, Int. J. Theor. Phys. **60**, 982 (2021).

[14] J. Zhang, J. Su, and Q. Zeng, Contributions of vector leptoquark to $\Xi_b \to \Xi_c\tau\bar{\nu}_\tau$ decay, Nucl. Phys. **B938**, 131 (2019).

[15] T. Mannel and G. A. Schuler, Semileptonic decays of bottom baryons at LEP, Phys. Lett. B **279**, 194 (1992).

[16] A. F. Falk and M. E. Peskin, Production, decay, and polarization of excited heavy hadrons, Phys. Rev. D **49**, 3320 (1994).

[17] M. Galanti, A. Giammanco, Y. Grossman, Y. Kats, E. Stamou, and J. Zupan, Heavy baryons as polarimeters at colliders, J. High Energy Phys. 11 (2015) 067.

[18] F. J. Botella, L. M. Garcia Martin, D. Marangotto, F. Martinez Vidal, A. Merli, N. Neri, A. Oyanguren, and J. Ruiz Vidal, On the search for the electric dipole moment of strange and charm baryons at LHC, Eur. Phys. J. C **77**, 181 (2017).

[19] E. Bagli *et al.*, Electromagnetic dipole moments of charged baryons with bent crystals at the LHC, Eur. Phys. J. C **77**, 828 (2017).

[20] A. S. Fomin *et al.*, Feasibility of measuring the magnetic dipole moments of the charm baryons at the LHC using bent crystals, J. High Energy Phys. 08 (2017) 120.

[21] D. Marangotto, Amplitude analysis and polarisation measurement of the Λ_c^+ baryon in $pK^-\pi^+$ final state for electromagnetic dipole moment experiment, Ph.D. thesis, Università degli studi di Milano, 2020, https://cds.cern.ch/record/2713231.

[22] A. S. Fomin, S. Barsuk, A. Yu. Korchin, E. Kou, V. A. Kovalchuk, M. Liul, A. Natochii, E. Niel, P. Robbe, and A. Stocchi, The prospect of charm quark magnetic moment determination, Eur. Phys. J. C **80**, 358 (2020).

[23] D. Mirarchi, A. S. Fomin, S. Redaelli, and W. Scandale, Layouts for fixed-target experiments and dipole moment measurements of short-lived baryons using bent crystals at the LHC, Eur. Phys. J. C **80**, 929 (2020).

[24] S. Aiola *et al.*, Progress towards the first measurement of charm baryon dipole moments, Phys. Rev. D **103**, 072003 (2020).

[25] R. Aaij *et al.* (LHCb Collaboration), Amplitude analysis of the $\Lambda_c^+ \to pK^-\pi^+$ decay and Λ_c^+ baryon polarization measurement in semileptonic beauty hadron decays, Phys. Rev. D **108**, 012023 (2023).

[26] A. A. Alves, Jr. *et al.* (LHCb Collaboration), The LHCb detector at the LHC, J. Instrum. **3**, S08005 (2008).

[27] LHCb Collaboration, LHCb detector performance, Int. J. Mod. Phys. A **30**, 1530022 (2015).

[28] V. V. Gligorov and M. Williams, Efficient, reliable and fast high-level triggering using a bonsai boosted decision tree, J. Instrum. **8**, P02013 (2013).

[29] T. Likhomanenko, P. Ilten, E. Khairullin, A. Rogozhnikov, A. Ustyuzhanin, and M. Williams, LHCb topological trigger reoptimization, J. Phys. Conf. Ser. **664**, 082025 (2015).

[30] R. Aaij *et al.* (LHCb Collaboration), Measurements of the Λ_b^0, Ξ_b^-, and Ω_b^- baryon masses, Phys. Rev. Lett. **110**, 182001 (2013).

[31] R. Aaij *et al.* (LHCb Collaboration), Precision measurement of D meson mass differences, J. High Energy Phys. 06 (2013) 065.

[32] T. Sjöstrand, S. Mrenna, and P. Skands, A brief introduction to PYTHIA 8.1, Comput. Phys. Commun. **178**, 852 (2008); PYTHIA 6.4 physics and manual, J. High Energy Phys. 05 (2006) 026.

[33] I. Belyaev *et al.*, Handling of the generation of primary events in Gauss, the LHCb simulation framework, J. Phys. Conf. Ser. **331**, 032047 (2011).

[34] D. J. Lange, The EvtGen particle decay simulation package, Nucl. Instrum. Methods Phys. Res., Sect. A **462**, 152 (2001).

[35] N. Davidson, T. Przedzinski, and Z. Was, PHOTOS interface in C++: Technical and physics documentation, Comput. Phys. Commun. **199**, 86 (2016).

[36] J. Allison *et al.* (Geant4 Collaboration), Geant4 developments and applications, IEEE Trans. Nucl. Sci. **53**, 270 (2006); S. Agostinelli *et al.* (Geant4 Collaboration), Geant4: A simulation toolkit, Nucl. Instrum. Methods Phys. Res., Sect. A **506**, 250 (2003).

[37] M. Clemencic, G. Corti, S. Easo, C. R. Jones, S. Miglioranzi, M. Pappagallo, and P. Robbe, The LHCb simulation application, Gauss: Design, evolution and experience, J. Phys. Conf. Ser. **331**, 032023 (2011).

[38] D. Müller, M. Clemencic, G. Corti, and M. Gersabeck, ReDecay: A novel approach to speed up the simulation at LHCb, Eur. Phys. J. C **78**, 1009 (2018).

[39] A. Poluektov, Kernel density estimation of a multidimensional efficiency profile, J. Instrum. **10**, P02011 (2015).

[40] A. Rogozhnikov, Reweighting with boosted decision trees, J. Phys. Conf. Ser. **762**, 012036 (2016).

[41] R. Aaij *et al.*, Selection and processing of calibration samples to measure the particle identification performance of the LHCb experiment in Run 2, Eur. Phys. J. Tech. Instrum. **6**, 1 (2019).

[42] L. Breiman, J. H. Friedman, R. A. Olshen, and C. J. Stone, *Classification and Regression Trees* (Wadsworth International Group, Belmont, CA, 1984).

[43] M. Pivk and F. R. Le Diberder, sPlot: A statistical tool to unfold data distributions, Nucl. Instrum. Methods Phys. Res., Sect. A **555**, 356 (2005).

[44] M. Jacob and G. C. Wick, On the general theory of collisions for particles with spin, Ann. Phys. (N.Y.) **7**, 404 (1959).

[45] D. Marangotto, Helicity amplitudes for generic multibody particle decays featuring multiple decay chains, Adv. High Energy Phys. **2020**, 6674595 (2020).

[46] TensorFlowAnalysis: A collection of useful functions and example scripts for performing amplitude fits using TensorFlow, https://gitlab.cern.ch/poluekt/TensorFlowAnalysis.

[47] M. Abadi *et al.*, TensorFlow: Large-scale machine learning on heterogeneous systems, Software available from https://www.tensorflow.org/ (2015).

[48] F. James and M. Roos, Minuit: A system for function minimization and analysis of the parameter errors and correlations, Comput. Phys. Commun. **10**, 343 (1975).

[49] R. Brun and F. Rademakers, ROOT: An object oriented data analysis framework, Nucl. Instrum. Methods Phys. Res., Sect. A **389**, 81 (1997).
[50] S. M. Flatté, Coupled-channel analysis of the $\pi\eta$ and $K\bar{K}$ systems near $K\bar{K}$ threshold, Phys. Lett. B **63**, 224 (1976).
[51] D. V. Bugg, The kappa in E791 data for $D \to K\pi\pi$, Phys. Lett. B **632**, 471 (2006).
[52] S. B. Yang *et al.* (Belle Collaboration), Observation of a threshold cusp at the $\Lambda\eta$ threshold in the pK^- mass spectrum with $\Lambda_c^+ \to pK^-\pi^+$ decays, Phys. Rev. D **108**, L031104 (2023).
[53] LHCb Collaboration (2025), https://cds.cern.ch/record/2939495.

R. Aaij,[38] A. S. W. Abdelmotteleb,[57] C. Abellan Beteta,[51] F. Abudinén,[57] T. Ackernley,[61] A. A. Adefisoye,[69] B. Adeva,[47] M. Adinolfi,[55] P. Adlarson,[82] C. Agapopoulou,[14] C. A. Aidala,[83] Z. Ajaltouni,[11] S. Akar,[66] K. Akiba,[38] P. Albicocco,[28] J. Albrecht,[19,b] F. Alessio,[49] Z. Aliouche,[63] P. Alvarez Cartelle,[56] R. Amalric,[16] S. Amato,[3] J. L. Amey,[55] Y. Amhis,[14] L. An,[6] L. Anderlini,[27] M. Andersson,[51] A. Andreianov,[44] P. Andreola,[51] M. Andreotti,[26] D. Andreou,[69] A. Anelli,[31,c] D. Ao,[7] F. Archilli,[37,d] M. Argenton,[26] S. Arguedas Cuendis,[9,49] A. Artamonov,[44] M. Artuso,[69] E. Aslanides,[13] R. Ataíde Da Silva,[50] M. Atzeni,[65] B. Audurier,[12] D. Bacher,[64] I. Bachiller Perea,[10] S. Bachmann,[22] M. Bachmayer,[50] J. J. Back,[57] P. Baladron Rodriguez,[47] V. Balagura,[15] A. Balboni,[26] W. Baldini,[26] L. Balzani,[19] H. Bao,[7] J. Baptista de Souza Leite,[61] C. Barbero Pretel,[47,12] M. Barbetti,[27] I. R. Barbosa,[70] R. J. Barlow,[63] M. Barnyakov,[25] S. Barsuk,[14] W. Barter,[59] M. Bartolini,[56] J. Bartz,[69] J. M. Basels,[17] S. Bashir,[40] G. Bassi,[35,e] B. Batsukh,[5] P. B. Battista,[14] A. Bay,[50] A. Beck,[57] M. Becker,[19] F. Bedeschi,[35] I. B. Bediaga,[2] N. A. Behling,[19] S. Belin,[47] K. Belous,[44] I. Belov,[29] I. Belyaev,[36] G. Benane,[13] G. Bencivenni,[28] E. Ben-Haim,[16] A. Berezhnoy,[44] R. Bernet,[51] S. Bernet Andres,[46] A. Bertolin,[33] C. Betancourt,[51] F. Betti,[59] J. Bex,[56] Ia. Bezshyiko,[51] J. Bhom,[41] M. S. Bieker,[19] N. V. Biesuz,[26] P. Billoir,[16] A. Biolchini,[38] M. Birch,[62] F. C. R. Bishop,[10] A. Bitadze,[63] A. Bizzeti,[27,f] T. Blake,[57] F. Blanc,[50] J. E. Blank,[19] S. Blusk,[69] V. Bocharnikov,[44] J. A. Boelhauve,[19] O. Boente Garcia,[15] T. Boettcher,[66] A. Bohare,[59] A. Boldyrev,[44] C. S. Bolognani,[79] R. Bolzonella,[26,g] R. B. Bonacci,[1] N. Bondar,[44] A. Bordelius,[49] F. Borgato,[33,h] S. Borghi,[63] M. Borsato,[31,c] J. T. Borsuk,[41] S. A. Bouchiba,[50] M. Bovill,[64] T. J. V. Bowcock,[61] A. Boyer,[49] C. Bozzi,[26] A. Brea Rodriguez,[50] N. Breer,[19] J. Brodzicka,[41] A. Brossa Gonzalo,[47,a] J. Brown,[61] D. Brundu,[32] E. Buchanan,[59] A. Buonaura,[51] L. Buonincontri,[33,h] A. T. Burke,[63] C. Burr,[49] J. S. Butter,[56] J. Buytaert,[49] W. Byczynski,[49] S. Cadeddu,[32] H. Cai,[74] A. Caillet,[16] R. Calabrese,[26,g] S. Calderon Ramirez,[9] L. Calefice,[45] S. Cali,[28] M. Calvi,[31,c] M. Calvo Gomez,[46] P. Camargo Magalhaes,[2,i] J. I. Cambon Bouzas,[47] P. Campana,[28] D. H. Campora Perez,[79] A. F. Campoverde Quezada,[7] S. Capelli,[31] L. Capriotti,[26] R. Caravaca-Mora,[9] A. Carbone,[25,j] L. Carcedo Salgado,[47] R. Cardinale,[29,k] A. Cardini,[32] P. Carniti,[31,c] L. Carus,[22] A. Casais Vidal,[65] R. Caspary,[22] G. Casse,[61] M. Cattaneo,[49] G. Cavallero,[26,49] V. Cavallini,[26,g] S. Celani,[22] D. Cervenkov,[64] S. Cesare,[30,l] A. J. Chadwick,[61] I. Chahrour,[83] M. Charles,[16] Ph. Charpentier,[49] E. Chatzianagnostou,[38] M. Chefdeville,[10] C. Chen,[13] S. Chen,[5] Z. Chen,[7] A. Chernov,[41] S. Chernyshenko,[53] X. Chiotopoulos,[79] V. Chobanova,[81] S. Cholak,[50] M. Chrzaszcz,[41] A. Chubykin,[44] V. Chulikov,[28] P. Ciambrone,[28] X. Cid Vidal,[47] G. Ciezarek,[49] P. Cifra,[49] P. E. L. Clarke,[59] M. Clemencic,[49] H. V. Cliff,[56] J. Closier,[49] C. Cocha Toapaxi,[22] V. Coco,[49] J. Cogan,[13] E. Cogneras,[11] L. Cojocariu,[43] S. Collaviti,[50] P. Collins,[49] T. Colombo,[49] M. Colonna,[19] A. Comerma-Montells,[45] L. Congedo,[24] A. Contu,[32] N. Cooke,[60] I. Corredoira,[47] A. Correia,[16] G. Corti,[49] J. Cottee Meldrum,[55] B. Couturier,[49] D. C. Craik,[51] M. Cruz Torres,[2,m] E. Curras Rivera,[50] R. Currie,[59] C. L. Da Silva,[68] S. Dadabaev,[44] L. Dai,[71] X. Dai,[6] E. Dall'Occo,[49] J. Dalseno,[47] C. D'Ambrosio,[49] J. Daniel,[11] A. Danilina,[44] P. d'Argent,[24] A. Davidson,[57] J. E. Davies,[63] A. Davis,[63] O. De Aguiar Francisco,[63] C. De Angelis,[32,n] F. De Benedetti,[49] J. de Boer,[38] K. De Bruyn,[78] S. De Capua,[63] M. De Cian,[22] U. De Freitas Carneiro Da Graca,[2,o] E. De Lucia,[28] J. M. De Miranda,[2] L. De Paula,[3] M. De Serio,[24,p] P. De Simone,[28] F. De Vellis,[19] J. A. de Vries,[79] F. Debernardis,[24] D. Decamp,[10] V. Dedu,[13] S. Dekkers,[1] L. Del Buono,[16] B. Delaney,[65] H.-P. Dembinski,[19] J. Deng,[8] V. Denysenko,[51] O. Deschamps,[11] F. Dettori,[32,n] B. Dey,[77] P. Di Nezza,[28] I. Diachkov,[44] S. Didenko,[44] S. Ding,[69] L. Dittmann,[22] V. Dobishuk,[53] A. D. Docheva,[60] C. Dong,[4,q] A. M. Donohoe,[23] F. Dordei,[32] A. C. dos Reis,[2]

A. D. Dowling,[69] W. Duan,[72] P. Duda,[80] M. W. Dudek,[41] L. Dufour,[49] V. Duk,[34] P. Durante,[49] M. M. Duras,[80] J. M. Durham,[68] O. D. Durmus,[77] A. Dziurda,[41] A. Dzyuba,[44] S. Easo,[58] E. Eckstein,[18] U. Egede,[1] A. Egorychev,[44] V. Egorychev,[44] S. Eisenhardt,[59] E. Ejopu,[63] L. Eklund,[82] M. Elashri,[66] J. Ellbracht,[19] S. Ely,[62] A. Ene,[43] J. Eschle,[69] S. Esen,[22] T. Evans,[63] F. Fabiano,[32,n] L. N. Falcao,[2] Y. Fan,[7] B. Fang,[7] L. Fantini,[34,49,r] M. Faria,[50] K. Farmer,[59] D. Fazzini,[31,c] L. Felkowski,[80] M. Feng,[5,7] M. Feo,[19] A. Fernandez Casani,[48] M. Fernandez Gomez,[47] A. D. Fernez,[67] F. Ferrari,[25,j] F. Ferreira Rodrigues,[3] M. Ferrillo,[51] M. Ferro-Luzzi,[49] S. Filippov,[44] R. A. Fini,[24] M. Fiorini,[26,g] M. Firlej,[40] K. L. Fischer,[64] D. S. Fitzgerald,[83] C. Fitzpatrick,[63] T. Fiutowski,[40] F. Fleuret,[15] M. Fontana,[25] L. F. Foreman,[63] R. Forty,[49] D. Foulds-Holt,[56] V. Franco Lima,[3] M. Franco Sevilla,[67] M. Frank,[49] E. Franzoso,[26,g] G. Frau,[63] C. Frei,[49] D. A. Friday,[63] J. Fu,[7] Q. Führing,[19,56,b] Y. Fujii,[1] T. Fulghesu,[16] E. Gabriel,[38] G. Galati,[24] M. D. Galati,[38] A. Gallas Torreira,[47] D. Galli,[25,j] S. Gambetta,[59] M. Gandelman,[3] P. Gandini,[30] B. Ganie,[63] H. Gao,[7] R. Gao,[64] T. Q. Gao,[56] Y. Gao,[8] Y. Gao,[6] Y. Gao,[8] L. M. Garcia Martin,[50] P. Garcia Moreno,[45] J. García Pardiñas,[49] P. Gardner,[67] K. G. Garg,[8] L. Garrido,[45] C. Gaspar,[49] R. E. Geertsema,[38] L. L. Gerken,[19] E. Gersabeck,[63] M. Gersabeck,[20] T. Gershon,[57] S. Ghizzo,[29,k] Z. Ghorbanimoghaddam,[55] L. Giambastiani,[33,h] F. I. Giasemis,[16,s] V. Gibson,[56] H. K. Giemza,[42] A. L. Gilman,[64] M. Giovannetti,[28] A. Gioventù,[45] L. Girardey,[63,58] P. Gironella Gironell,[45] C. Giugliano,[26,g] M. A. Giza,[41] E. L. Gkougkousis,[62] F. C. Glaser,[14,22] V. V. Gligorov,[16,49] C. Göbel,[70] E. Golobardes,[46] D. Golubkov,[44] A. Golutvin,[62,49,44] S. Gomez Fernandez,[45] W. Gomulka,[40] F. Goncalves Abrantes,[64] M. Goncerz,[41] G. Gong,[4,q] J. A. Gooding,[19] I. V. Gorelov,[44] C. Gotti,[31] J. P. Grabowski,[18] L. A. Granado Cardoso,[49] E. Graugés,[45] E. Graverini,[50,t] L. Grazette,[57] G. Graziani,[27] A. T. Grecu,[43] L. M. Greeven,[38] N. A. Grieser,[66] L. Grillo,[60] S. Gromov,[44] C. Gu,[15] M. Guarise,[26] L. Guerry,[11] M. Guittiere,[14] V. Guliaeva,[44] P. A. Günther,[22] A.-K. Guseinov,[50] E. Gushchin,[44] Y. Guz,[6,49,44] T. Gys,[49] K. Habermann,[18] T. Hadavizadeh,[1] C. Hadjivasiliou,[67] G. Haefeli,[50] C. Haen,[49] M. Hajheidari,[49] G. Hallett,[57] M. M. Halvorsen,[49] P. M. Hamilton,[67] J. Hammerich,[61] Q. Han,[8] X. Han,[22,49] S. Hansmann-Menzemer,[22] L. Hao,[7] N. Harnew,[64] T. H. Harris,[1] M. Hartmann,[14] S. Hashmi,[40] J. He,[7,u] F. Hemmer,[49] C. Henderson,[66] R. D. L. Henderson,[1,57] A. M. Hennequin,[49] K. Hennessy,[61] L. Henry,[50] J. Herd,[62] P. Herrero Gascon,[22] J. Heuel,[17] A. Hicheur,[3] G. Hijano Mendizabal,[51] J. Horswill,[63] R. Hou,[8] Y. Hou,[11] N. Howarth,[61] J. Hu,[72] W. Hu,[6] X. Hu,[4,q] W. Huang,[7] W. Hulsbergen,[38] R. J. Hunter,[57] M. Hushchyn,[44] D. Hutchcroft,[61] M. Idzik,[40] D. Ilin,[44] P. Ilten,[66] A. Inglessi,[44] A. Iniukhin,[44] A. Ishteev,[44] K. Ivshin,[44] R. Jacobsson,[49] H. Jage,[17] S. J. Jaimes Elles,[75,48,49] S. Jakobsen,[49] E. Jans,[38] B. K. Jashal,[48] A. Jawahery,[67,49] V. Jevtic,[19,b] E. Jiang,[67] X. Jiang,[5,7] Y. Jiang,[7] Y. J. Jiang,[6] M. John,[64] A. John Rubesh Rajan,[23] D. Johnson,[54] C. R. Jones,[56] T. P. Jones,[57] S. Joshi,[42] B. Jost,[49] J. Juan Castella,[56] N. Jurik,[49] I. Juszczak,[41] D. Kaminaris,[50] S. Kandybei,[52] M. Kane,[59] Y. Kang,[4,q] C. Kar,[11] M. Karacson,[49] D. Karpenkov,[44] A. Kauniskangas,[50] J. W. Kautz,[66] M. K. Kazanecki,[41] F. Keizer,[49] M. Kenzie,[56] T. Ketel,[38] B. Khanji,[69] A. Kharisova,[44] S. Kholodenko,[35,49] G. Khreich,[14] T. Kirn,[17] V. S. Kirsebom,[31,c] O. Kitouni,[65] S. Klaver,[39] N. Kleijne,[35,e] K. Klimaszewski,[42] M. R. Kmiec,[42] S. Koliiev,[53] L. Kolk,[19] A. Konoplyannikov,[44] P. Kopciewicz,[40,49] P. Koppenburg,[38] M. Korolev,[44] I. Kostiuk,[38] O. Kot,[53] S. Kotriakhova, A. Kozachuk,[44] P. Kravchenko,[44] L. Kravchuk,[44] M. Kreps,[57] P. Krokovny,[44] W. Krupa,[69] W. Krzemien,[42] O. Kshyvanskyi,[53] S. Kubis,[80] M. Kucharczyk,[41] V. Kudryavtsev,[44] E. Kulikova,[44] A. Kupsc,[82] B. Kutsenko,[13] D. Lacarrere,[49] P. Laguarta Gonzalez,[45] A. Lai,[32] A. Lampis,[32] D. Lancierini,[56] C. Landesa Gomez,[47] J. J. Lane,[1] R. Lane,[55] G. Lanfranchi,[28] C. Langenbruch,[22] J. Langer,[19] O. Lantwin,[44] T. Latham,[57] F. Lazzari,[35,t] C. Lazzeroni,[54] R. Le Gac,[13] H. Lee,[61] R. Lefèvre,[11] A. Leflat,[44] S. Legotin,[44] M. Lehuraux,[57] E. Lemos Cid,[49] O. Leroy,[13] T. Lesiak,[41] E. D. Lesser,[49] B. Leverington,[22] A. Li,[4,q] C. Li,[13] H. Li,[72] K. Li,[8] L. Li,[63] M. Li,[8] P. Li,[7] P.-R. Li,[73] Q. Li,[5,7] S. Li,[8] T. Li,[5,v] T. Li,[72] Y. Li,[8] Y. Li,[5] Z. Lian,[4,q] X. Liang,[69] S. Libralon,[48] C. Lin,[7] T. Lin,[58] R. Lindner,[49] H. Linton,[62] V. Lisovskyi,[50] R. Litvinov,[32,49] F. L. Liu,[1] G. Liu,[72] K. Liu,[73] S. Liu,[5,7] W. Liu,[8] Y. Liu,[59] Y. Liu,[73] Y. L. Liu,[62] A. Lobo Salvia,[45] A. Loi,[32] T. Long,[56] J. H. Lopes,[3] A. Lopez Huertas,[45] S. López Soliño,[47] Q. Lu,[15] C. Lucarelli,[27] D. Lucchesi,[33,h] M. Lucio Martinez,[79] V. Lukashenko,[38,53] Y. Luo,[6] A. Lupato,[33,w] E. Luppi,[26,g] K. Lynch,[23] X.-R. Lyu,[7] G. M. Ma,[4,q] S. Maccolini,[19] F. Machefert,[14] F. Maciuc,[43] B. Mack,[69] I. Mackay,[64] L. M. Mackey,[69] L. R. Madhan Mohan,[56] M. J. Madurai,[54] A. Maevskiy,[44] D. Magdalinski,[38] D. Maisuzenko,[44] M. W. Majewski,[40] J. J. Malczewski,[41] S. Malde,[64] L. Malentacca,[49]

A. Malinin,[44] T. Maltsev,[44] G. Manca,[32,n] G. Mancinelli,[13] C. Mancuso,[30,14,l] R. Manera Escalero,[45] F. M. Manganella,[37] D. Manuzzi,[25] D. Marangotto,[30,l] J. F. Marchand,[10] R. Marchevski,[50] U. Marconi,[25] E. Mariani,[16] S. Mariani,[49] C. Marin Benito,[45,49] J. Marks,[22] A. M. Marshall,[55] L. Martel,[64] G. Martelli,[34,r] G. Martellotti,[36] L. Martinazzoli,[49] M. Martinelli,[31,c] D. Martinez Gomez,[78] D. Martinez Santos,[81] F. Martinez Vidal,[48] A. Martorell i Granollers,[46] A. Massafferri,[2] R. Matev,[49] A. Mathad,[49] V. Matiunin,[44] C. Matteuzzi,[69] K. R. Mattioli,[15] A. Mauri,[62] E. Maurice,[15] J. Mauricio,[45] P. Mayencourt,[50] J. Mazorra de Cos,[48] M. Mazurek,[42] M. McCann,[62] L. Mcconnell,[23] T. H. McGrath,[63] N. T. McHugh,[60] A. McNab,[63] R. McNulty,[23] B. Meadows,[66] G. Meier,[19] D. Melnychuk,[42] F. M. Meng,[4,q] M. Merk,[38,79] A. Merli,[50] L. Meyer Garcia,[67] D. Miao,[5,7] H. Miao,[7] M. Mikhasenko,[76] D. A. Milanes,[75] A. Minotti,[31,c] E. Minucci,[28] T. Miralles,[11] B. Mitreska,[19] D. S. Mitzel,[19] A. Modak,[58] R. A. Mohammed,[64] R. D. Moise,[17] S. Mokhnenko,[44] E. F. Molina Cardenas,[83] T. Mombächer,[49] M. Monk,[57,1] S. Monteil,[11] A. Morcillo Gomez,[47] G. Morello,[28] M. J. Morello,[35,e] M. P. Morgenthaler,[22] J. Moron,[40] W. Morren,[38] A. B. Morris,[49] A. G. Morris,[13] R. Mountain,[69] H. Mu,[4,q] Z. M. Mu,[6] E. Muhammad,[57] F. Muheim,[59] M. Mulder,[78] K. Müller,[51] F. Muñoz-Rojas,[9] R. Murta,[62] P. Naik,[61] T. Nakada,[50] R. Nandakumar,[58] T. Nanut,[49] I. Nasteva,[3] M. Needham,[59] N. Neri,[30,l] S. Neubert,[18] N. Neufeld,[49] P. Neustroev,[44] J. Nicolini,[19,14] D. Nicotra,[79] E. M. Niel,[49] N. Nikitin,[44] Q. Niu,[73] P. Nogarolli,[3] P. Nogga,[18] C. Normand,[55] J. Novoa Fernandez,[47] G. Nowak,[66] C. Nunez,[83] H. N. Nur,[60] A. Oblakowska-Mucha,[40] V. Obraztsov,[44] T. Oeser,[17] S. Okamura,[26,g] A. Okhotnikov,[44] O. Okhrimenko,[53] R. Oldeman,[32,n] F. Oliva,[59] M. Olocco,[19] C. J. G. Onderwater,[79] R. H. O'Neil,[59] D. Osthues,[19] J. M. Otalora Goicochea,[3] P. Owen,[51] A. Oyanguren,[48] O. Ozcelik,[59] F. Paciolla,[35,x] A. Padee,[42] K. O. Padeken,[18] B. Pagare,[57] P. R. Pais,[22] T. Pajero,[49] A. Palano,[24] M. Palutan,[28] X. Pan,[4,q] G. Panshin,[44] L. Paolucci,[57] A. Papanestis,[58,49] M. Pappagallo,[24,p] L. L. Pappalardo,[26,g] C. Pappenheimer,[66] C. Parkes,[63] D. Parmar,[76] B. Passalacqua,[26,g] G. Passaleva,[27] D. Passaro,[35,e] A. Pastore,[24] M. Patel,[62] J. Patoc,[64] C. Patrignani,[25,j] A. Paul,[69] C. J. Pawley,[79] A. Pellegrino,[38] J. Peng,[5,7] M. Pepe Altarelli,[28] S. Perazzini,[25] D. Pereima,[44] H. Pereira Da Costa,[68] A. Pereiro Castro,[47] P. Perret,[11] A. Perrevoort,[78] A. Perro,[49,13] K. Petridis,[55] A. Petrolini,[29,k] J. P. Pfaller,[66] H. Pham,[69] L. Pica,[35,e] M. Piccini,[34] L. Piccolo,[32] B. Pietrzyk,[10] G. Pietrzyk,[14] D. Pinci,[36] F. Pisani,[49] M. Pizzichemi,[31,49,c] V. M. Placinta,[43] M. Plo Casasus,[47] T. Poeschl,[49] F. Polci,[16,49] M. Poli Lener,[28] A. Poluektov,[13] N. Polukhina,[44] I. Polyakov,[44] E. Polycarpo,[3] S. Ponce,[49] D. Popov,[7] S. Poslavskii,[44] K. Prasanth,[59] C. Prouve,[81] D. Provenzano,[32,n] V. Pugatch,[53] G. Punzi,[35,t] S. Qasim,[51] Q. Q. Qian,[6] W. Qian,[7] N. Qin,[4,q] S. Qu,[4,q] R. Quagliani,[49] R. I. Rabadan Trejo,[57] J. H. Rademacker,[55] M. Rama,[35] M. Ramírez García,[83] V. Ramos De Oliveira,[70] M. Ramos Pernas,[57] M. S. Rangel,[3] F. Ratnikov,[44] G. Raven,[39] M. Rebollo De Miguel,[48] F. Redi,[30,w] J. Reich,[55] F. Reiss,[63] Z. Ren,[7] P. K. Resmi,[64] R. Ribatti,[50] G. Ricart,[15,12] D. Riccardi,[35,e] S. Ricciardi,[58] K. Richardson,[65] M. Richardson-Slipper,[59] K. Rinnert,[61] P. Robbe,[14,49] G. Robertson,[60] E. Rodrigues,[61] A. Rodriguez Alvarez,[45] E. Rodriguez Fernandez,[47] J. A. Rodriguez Lopez,[75] E. Rodriguez Rodriguez,[47] J. Roensch,[19] A. Rogachev,[44] A. Rogovskiy,[58] D. L. Rolf,[49] P. Roloff,[49] V. Romanovskiy,[66] A. Romero Vidal,[47] G. Romolini,[26] F. Ronchetti,[50] T. Rong,[6] M. Rotondo,[28] S. R. Roy,[22] M. S. Rudolph,[69] M. Ruiz Diaz,[22] R. A. Ruiz Fernandez,[47] J. Ruiz Vidal,[82,y] A. Ryzhikov,[44] J. Ryzka,[40] J. J. Saavedra-Arias,[9] J. J. Saborido Silva,[47] R. Sadek,[15] N. Sagidova,[44] D. Sahoo,[77] N. Sahoo,[54] B. Saitta,[32,n] M. Salomoni,[31,49,c] I. Sanderswood,[48] R. Santacesaria,[36] C. Santamarina Rios,[47] M. Santimaria,[28,49] L. Santoro,[2] E. Santovetti,[37] A. Saputi,[26,49] D. Saranin,[44] A. Sarnatskiy,[78] G. Sarpis,[59] M. Sarpis,[63] C. Satriano,[36,z] A. Satta,[37] M. Saur,[6] D. Savrina,[44] H. Sazak,[17] F. Sborzacchi,[49,28] L. G. Scantlebury Smead,[64] A. Scarabotto,[19] S. Schael,[17] S. Scherl,[61] M. Schiller,[60] H. Schindler,[49] M. Schmelling,[21] B. Schmidt,[49] S. Schmitt,[17] H. Schmitz,[18] O. Schneider,[50] A. Schopper,[49] N. Schulte,[19] S. Schulte,[50] M. H. Schune,[14] R. Schwemmer,[49] G. Schwering,[17] B. Sciascia,[28] A. Sciuccati,[49] S. Sellam,[47] A. Semennikov,[44] T. Senger,[51] M. Senghi Soares,[39] A. Sergi,[29,k] N. Serra,[51] L. Sestini,[33] A. Seuthe,[19] Y. Shang,[6] D. M. Shangase,[83] M. Shapkin,[44] R. S. Sharma,[69] I. Shchemerov,[44] L. Shchutska,[50] T. Shears,[61] L. Shekhtman,[44] Z. Shen,[6] S. Sheng,[5,7] V. Shevchenko,[44] B. Shi,[7] Q. Shi,[7] Y. Shimizu,[14] E. Shmanin,[25] R. Shorkin,[44] J. D. Shupperd,[69] R. Silva Coutinho,[69] G. Simi,[33,h] S. Simone,[24,p] N. Skidmore,[57] T. Skwarnicki,[69] M. W. Slater,[54] J. C. Smallwood,[64] E. Smith,[65] K. Smith,[68] M. Smith,[62] A. Snoch,[38] L. Soares Lavra,[59] M. D. Sokoloff,[66] F. J. P. Soler,[60] A. Solomin,[44,55] A. Solovev,[44] I. Solovyev,[44]

N. S. Sommerfeld,[18] R. Song,[1] Y. Song,[50] Y. Song,[4,q] Y. S. Song,[6] F. L. Souza De Almeida,[69] B. Souza De Paula,[3] E. Spadaro Norella,[29,k] E. Spedicato,[25] J. G. Speer,[19] E. Spiridenkov,[44] P. Spradlin,[60] V. Sriskaran,[49] F. Stagni,[49] M. Stahl,[49] S. Stahl,[49] S. Stanislaus,[64] E. N. Stein,[49] O. Steinkamp,[51] O. Stenyakin,[44] H. Stevens,[19] D. Strekalina,[44] Y. Su,[7] F. Suljik,[64] J. Sun,[32] L. Sun,[74] D. Sundfeld,[2] W. Sutcliffe,[51] P. N. Swallow,[54] K. Swientek,[40] F. Swystun,[56] A. Szabelski,[42] T. Szumlak,[40] Y. Tan,[4,q] Y. Tang,[74] M. D. Tat,[64] A. Terentev,[44] F. Terzuoli,[35,49,x] F. Teubert,[49] E. Thomas,[49] D. J. D. Thompson,[54] H. Tilquin,[62] V. Tisserand,[11] S. T'Jampens,[10] M. Tobin,[5,49] L. Tomassetti,[26,g] G. Tonani,[30,49,l] X. Tong,[6] D. Torres Machado,[2] L. Toscano,[19] D. Y. Tou,[4,q] C. Trippl,[46] G. Tuci,[22] N. Tuning,[38] L. H. Uecker,[22] A. Ukleja,[40] D. J. Unverzagt,[22] B. Urbach,[59] E. Ursov,[44] A. Usachov,[39] A. Ustyuzhanin,[44] U. Uwer,[22] V. Vagnoni,[25] V. Valcarce Cadenas,[47] G. Valenti,[25] N. Valls Canudas,[49] H. Van Hecke,[68] E. van Herwijnen,[62] C. B. Van Hulse,[47,aa] R. Van Laak,[50] M. van Veghel,[38] G. Vasquez,[51] R. Vazquez Gomez,[45] P. Vazquez Regueiro,[47] C. Vázquez Sierra,[47] S. Vecchi,[26] J. J. Velthuis,[55] M. Veltri,[27,bb] A. Venkateswaran,[50] M. Verdoglia,[32] M. Vesterinen,[57] D. Vico Benet,[64] P. Vidrier Villalba,[45] M. Vieites Diaz,[49] X. Vilasis-Cardona,[46] E. Vilella Figueras,[61] A. Villa,[25] P. Vincent,[16] F. C. Volle,[54] D. vom Bruch,[13] N. Voropaev,[44] K. Vos,[79] C. Vrahas,[59] J. Wagner,[19] J. Walsh,[35] E. J. Walton,[1,57] G. Wan,[6] C. Wang,[22] G. Wang,[8] H. Wang,[73] J. Wang,[6] J. Wang,[5] J. Wang,[4,q] J. Wang,[74] M. Wang,[30] N. W. Wang,[7] R. Wang,[55] X. Wang,[8] X. Wang,[72] X. W. Wang,[62] Y. Wang,[6] Y. H. Wang,[73] Z. Wang,[14] Z. Wang,[4,q] Z. Wang,[30] J. A. Ward,[57,1] M. Waterlaat,[49] N. K. Watson,[54] D. Websdale,[62] Y. Wei,[6] J. Wendel,[81] B. D. C. Westhenry,[55] C. White,[56] M. Whitehead,[60] E. Whiter,[54] A. R. Wiederhold,[63] D. Wiedner,[19] G. Wilkinson,[64] M. K. Wilkinson,[66] M. Williams,[65] M. J. Williams,[49] M. R. J. Williams,[59] R. Williams,[56] Z. Williams,[55] F. F. Wilson,[58] M. Winn,[12] W. Wislicki,[42] M. Witek,[41] L. Witola,[22] G. Wormser,[14] S. A. Wotton,[56] H. Wu,[69] J. Wu,[8] X. Wu,[74] Y. Wu,[6] Z. Wu,[7] K. Wyllie,[49] S. Xian,[72] Z. Xiang,[5] Y. Xie,[8] A. Xu,[35] J. Xu,[7] L. Xu,[4,q] L. Xu,[4,q] M. Xu,[57] Z. Xu,[49] Z. Xu,[7] Z. Xu,[5] K. Yang,[62] S. Yang,[7] X. Yang,[6] Y. Yang,[29,k] Z. Yang,[6] V. Yeroshenko,[14] H. Yeung,[63] H. Yin,[8] X. Yin,[7] C. Y. Yu,[6] J. Yu,[71] X. Yuan,[5] Y Yuan,[5,7] E. Zaffaroni,[50] M. Zavertyaev,[21] M. Zdybal,[41] F. Zenesini,[25,j] C. Zeng,[5,7] M. Zeng,[4,q] C. Zhang,[6] D. Zhang,[8] J. Zhang,[7] L. Zhang,[4,q] S. Zhang,[71] S. Zhang,[64] Y. Zhang,[6] Y. Z. Zhang,[4,q] Y. Zhao,[22] A. Zharkova,[44] A. Zhelezov,[22] S. Z. Zheng,[6] X. Z. Zheng,[4,q] Y. Zheng,[7] T. Zhou,[6] X. Zhou,[8] Y. Zhou,[7] V. Zhovkovska,[57] L. Z. Zhu,[7] X. Zhu,[4,q] X. Zhu,[8] V. Zhukov,[17] J. Zhuo,[48] Q. Zou,[5,7] D. Zuliani,[33,h] and G. Zunica[50]

(LHCb Collaboration)

[1]*School of Physics and Astronomy, Monash University, Melbourne, Australia*
[2]*Centro Brasileiro de Pesquisas Físicas (CBPF), Rio de Janeiro, Brazil*
[3]*Universidade Federal do Rio de Janeiro (UFRJ), Rio de Janeiro, Brazil*
[4]*Department of Engineering Physics, Tsinghua University, Beijing, China*
[5]*Institute of High Energy Physics (IHEP), Beijing, China*
[6]*School of Physics State Key Laboratory of Nuclear Physics and Technology, Peking University, Beijing, China*
[7]*University of Chinese Academy of Sciences, Beijing, China*
[8]*Institute of Particle Physics, Central China Normal University, Wuhan, Hubei, China*
[9]*Consejo Nacional de Rectores (CONARE), San Jose, Costa Rica*
[10]*Université Savoie Mont Blanc, CNRS, IN2P3-LAPP, Annecy, France*
[11]*Université Clermont Auvergne, CNRS/IN2P3, LPC, Clermont-Ferrand, France*
[12]*Université Paris-Saclay, Centre d'Etudes de Saclay (CEA), IRFU, Saclay, France, Gif-Sur-Yvette, France*
[13]*Aix Marseille Univ, CNRS/IN2P3, CPPM, Marseille, France*
[14]*Université Paris-Saclay, CNRS/IN2P3, IJCLab, Orsay, France*
[15]*Laboratoire Leprince-Ringuet, CNRS/IN2P3, Ecole Polytechnique, Institut Polytechnique de Paris, Palaiseau, France*
[16]*LPNHE, Sorbonne Université, Paris Diderot Sorbonne Paris Cité, CNRS/IN2P3, Paris, France*
[17]*I. Physikalisches Institut, RWTH Aachen University, Aachen, Germany*
[18]*Universität Bonn—Helmholtz-Institut für Strahlen und Kernphysik, Bonn, Germany*
[19]*Fakultät Physik, Technische Universität Dortmund, Dortmund, Germany*

[20]*Physikalisches Institut, Albert-Ludwigs-Universität Freiburg, Freiburg, Germany*
[21]*Max-Planck-Institut für Kernphysik (MPIK), Heidelberg, Germany*
[22]*Physikalisches Institut, Ruprecht-Karls-Universität Heidelberg, Heidelberg, Germany*
[23]*School of Physics, University College Dublin, Dublin, Ireland*
[24]*INFN Sezione di Bari, Bari, Italy*
[25]*INFN Sezione di Bologna, Bologna, Italy*
[26]*INFN Sezione di Ferrara, Ferrara, Italy*
[27]*INFN Sezione di Firenze, Firenze, Italy*
[28]*INFN Laboratori Nazionali di Frascati, Frascati, Italy*
[29]*INFN Sezione di Genova, Genova, Italy*
[30]*INFN Sezione di Milano, Milano, Italy*
[31]*INFN Sezione di Milano-Bicocca, Milano, Italy*
[32]*INFN Sezione di Cagliari, Monserrato, Italy*
[33]*INFN Sezione di Padova, Padova, Italy*
[34]*INFN Sezione di Perugia, Perugia, Italy*
[35]*INFN Sezione di Pisa, Pisa, Italy*
[36]*INFN Sezione di Roma La Sapienza, Roma, Italy*
[37]*INFN Sezione di Roma Tor Vergata, Roma, Italy*
[38]*Nikhef National Institute for Subatomic Physics, Amsterdam, Netherlands*
[39]*Nikhef National Institute for Subatomic Physics and VU University Amsterdam, Amsterdam, Netherlands*
[40]*AGH—University of Krakow, Faculty of Physics and Applied Computer Science, Kraków, Poland*
[41]*Henryk Niewodniczanski Institute of Nuclear Physics Polish Academy of Sciences, Kraków, Poland*
[42]*National Center for Nuclear Research (NCBJ), Warsaw, Poland*
[43]*Horia Hulubei National Institute of Physics and Nuclear Engineering, Bucharest-Magurele, Romania*
[44]*Authors affiliated with an institute formerly covered by a cooperation agreement with CERN*
[45]*ICCUB, Universitat de Barcelona, Barcelona, Spain*
[46]*La Salle, Universitat Ramon Llull, Barcelona, Spain*
[47]*Instituto Galego de Física de Altas Enerxías (IGFAE), Universidade de Santiago de Compostela, Santiago de Compostela, Spain*
[48]*Instituto de Fisica Corpuscular, Centro Mixto Universidad de Valencia—CSIC, Valencia, Spain*
[49]*European Organization for Nuclear Research (CERN), Geneva, Switzerland*
[50]*Institute of Physics, Ecole Polytechnique Fédérale de Lausanne (EPFL), Lausanne, Switzerland*
[51]*Physik-Institut, Universität Zürich, Zürich, Switzerland*
[52]*NSC Kharkiv Institute of Physics and Technology (NSC KIPT), Kharkiv, Ukraine*
[53]*Institute for Nuclear Research of the National Academy of Sciences (KINR), Kyiv, Ukraine*
[54]*School of Physics and Astronomy, University of Birmingham, Birmingham, United Kingdom*
[55]*H.H. Wills Physics Laboratory, University of Bristol, Bristol, United Kingdom*
[56]*Cavendish Laboratory, University of Cambridge, Cambridge, United Kingdom*
[57]*Department of Physics, University of Warwick, Coventry, United Kingdom*
[58]*STFC Rutherford Appleton Laboratory, Didcot, United Kingdom*
[59]*School of Physics and Astronomy, University of Edinburgh, Edinburgh, United Kingdom*
[60]*School of Physics and Astronomy, University of Glasgow, Glasgow, United Kingdom*
[61]*Oliver Lodge Laboratory, University of Liverpool, Liverpool, United Kingdom*
[62]*Imperial College London, London, United Kingdom*
[63]*Department of Physics and Astronomy, University of Manchester, Manchester, United Kingdom*
[64]*Department of Physics, University of Oxford, Oxford, United Kingdom*
[65]*Massachusetts Institute of Technology, Cambridge, Massachusetts, USA*
[66]*University of Cincinnati, Cincinnati, Ohio, USA*
[67]*University of Maryland, College Park, Maryland, USA*
[68]*Los Alamos National Laboratory (LANL), Los Alamos, New Mexico, USA*
[69]*Syracuse University, Syracuse, New York, USA*
[70]*Pontifícia Universidade Católica do Rio de Janeiro (PUC-Rio), Rio de Janeiro, Brazil (associated with Universidade Federal do Rio de Janeiro (UFRJ), Rio de Janeiro, Brazil)*
[71]*School of Physics and Electronics, Hunan University, Changsha City, China (associated with Institute of Particle Physics, Central China Normal University, Wuhan, Hubei, China)*
[72]*Guangdong Provincial Key Laboratory of Nuclear Science, Guangdong-Hong Kong Joint Laboratory of Quantum Matter, Institute of Quantum Matter, South China Normal University, Guangzhou, China (associated with Department of Engineering Physics, Tsinghua University, Beijing, China)*
[73]*Lanzhou University, Lanzhou, China (associated with Institute Of High Energy Physics (IHEP), Beijing, China)*

[74]School of Physics and Technology, Wuhan University, Wuhan, China (associated with Department of Engineering Physics, Tsinghua University, Beijing, China)
[75]Departamento de Fisica, Universidad Nacional de Colombia, Bogota, Colombia (associated with LPNHE, Sorbonne Université, Paris Diderot Sorbonne Paris Cité, CNRS/IN2P3, Paris, France)
[76]Ruhr Universitaet Bochum, Fakultaet für Physik und Astronomie, Bochum, Germany (associated with Fakultät Physik, Technische Universität Dortmund, Dortmund, Germany)
[77]Eotvos Lorand University, Budapest, Hungary (associated with European Organization for Nuclear Research (CERN), Geneva, Switzerland)
[78]Van Swinderen Institute, University of Groningen, Groningen, Netherlands (associated with Nikhef National Institute for Subatomic Physics, Amsterdam, Netherlands)
[79]Universiteit Maastricht, Maastricht, Netherlands (associated with Nikhef National Institute for Subatomic Physics, Amsterdam, Netherlands)
[80]Tadeusz Kosciuszko Cracow University of Technology, Cracow, Poland (associated with Henryk Niewodniczanski Institute of Nuclear Physics Polish Academy of Sciences, Kraków, Poland)
[81]Universidade da Coruña, A Coruña, Spain (associated with La Salle, Universitat Ramon Llull, Barcelona, Spain)
[82]Department of Physics and Astronomy, Uppsala University, Uppsala, Sweden (associated with School of Physics and Astronomy, University of Glasgow, Glasgow, United Kingdom)
[83]University of Michigan, Ann Arbor, Michigan, USA (associated with Syracuse University, Syracuse, New York, USA)

[a]Deceased.
[b]Also at Lamarr Institute for Machine Learning and Artificial Intelligence, Dortmund, Germany.
[c]Also at Università degli Studi di Milano-Bicocca, Milano, Italy.
[d]Also at Università di Roma Tor Vergata, Roma, Italy.
[e]Also at Scuola Normale Superiore, Pisa, Italy.
[f]Also at Università di Modena e Reggio Emilia, Modena, Italy.
[g]Also at Università di Ferrara, Ferrara, Italy.
[h]Also at Università di Padova, Padova, Italy.
[i]Also at Universidade Estadual de Campinas (UNICAMP), Campinas, Brazil.
[j]Also at Università di Bologna, Bologna, Italy.
[k]Also at Università di Genova, Genova, Italy.
[l]Also at Università degli Studi di Milano, Milano, Italy.
[m]Also at Universidad Nacional Autónoma de Honduras, Tegucigalpa, Honduras.
[n]Also at Università di Cagliari, Cagliari, Italy.
[o]Also at Centro Federal de Educacão Tecnológica Celso Suckow da Fonseca, Rio De Janeiro, Brazil.
[p]Also at Università di Bari, Bari, Italy.
[q]Also at Center for High Energy Physics, Tsinghua University, Beijing, China.
[r]Also at Università di Perugia, Perugia, Italy.
[s]Also at LIP6, Sorbonne Université, Paris, France.
[t]Also at Università di Pisa, Pisa, Italy.
[u]Also at Hangzhou Institute for Advanced Study, UCAS, Hangzhou, China.
[v]Also at School of Physics and Electronics, Henan University, Kaifeng, China.
[w]Also at Università di Bergamo, Bergamo, Italy.
[x]Also at Università di Siena, Siena, Italy.
[y]Also at Department of Physics/Division of Particle Physics, Lund, Sweden.
[z]Also at Università della Basilicata, Potenza, Italy.
[aa]Also at Universidad de Alcalá, Alcalá de Henares, Spain.
[bb]Also at Università di Urbino, Urbino, Italy.